(4)

David Taylor Research Center

Bethesda, MD 20084-5000

DTRC-90/013 May 1990

Ship Hydromechanics Department
Research and Development Report

Prediction of Propeller Blade Pressure Distribution with a Panel Method

by

Cheng I. Yang

DTRC-90/013 Prediction of Propeller Blade Pressure Distribution with a Panel Method

MAJOR DTRC TECHNICAL COMPONENTS

CODE 011 DIRECTOR OF TECHNOLOGY, PLANS AND ASSESSMENT

12 SHIP SYSTEMS INTEGRATION DEPARTMENT

14 SHIP ELECTROMAGNETIC SIGNATURES DEPARTMENT

15 SHIP HYDROMECHANICS DEPARTMENT

16 AVIATION DEPARTMENT

17 SHIP STRUCTURES AND PROTECTION DEPARTMENT

18 COMPUTATION, MATHEMATICS & LOGISTICS DEPARTMENT

19 SHIP ACOUSTICS DEPARTMENT

27 PROPULSION AND AUXILIARY SYSTEMS DEPARTMENT

28 SHIP MATERIALS ENGINEERING DEPARTMENT

DTRC ISSUES THREE TYPES OF REPORTS:

1. **DTRC reports, a formal series,** contain information of permanent technical value. They carry a consecutive numerical identification regardless of their classification or the originating department.

2. **Departmental reports, a semiformal series,** contain information of a preliminary, temporary, or proprietary nature or of limited interest or significance. They carry a departmental alphanumerical identification.

3. **Technical memoranda, an informal series,** contain technical documentation of limited use and interest. They are primarily working papers intended for internal use. They carry an identifying number which indicates their type and the numerical code of the originating department. Any distribution outside DTRC must be approved by the head of the originating department on a case-by-case basis.

NDW-DTNSRDC 5602/51 (Rev. 2-88)

REPORT DOCUMENTATION PAGE

1a. REPORT SECURITY CLASSIFICATION Unclassified	1b. RESTRICTIVE MARKINGS
2a. SECURITY CLASSIFICATION AUTHORITY	3. DISTRIBUTION/AVAILABILITY OF REPORT Approved for Public Release; Distribution is Unlimited.
2b. DECLASSIFICATION/DOWNGRADING SCHEDULE	
4. PERFORMING ORGANIZATION REPORT NUMBER(S) DTRC-90/013	5. MONITORING ORGANIZATION REPORT NUMBER(S)
6a. NAME OF PERFORMING ORGANIZATION David Taylor Research Center 6b. OFFICE SYMBOL (If applicable) Code 1544	7a. NAME OF MONITORING ORGANIZATION
6c. ADDRESS (City, State, and ZIP Code) Bethesda, MD 20084-5000	7b. ADDRESS (City, State, and ZIP Code)
8a. NAME OF FUNDING/SPONSORING ORGANIZATION 8b. OFFICE SYMBOL (If applicable)	9. PROCUREMENT INSTRUMENT IDENTIFICATION NUMBER
8c. ADDRESS (City, State, and ZIP Code)	10. SOURCE OF FUNDING NUMBERS PROGRAM ELEMENT NO. 62543N; PROJECT NO.; TASK NO.; WORK UNIT ACCESSION NO.
11. TITLE (Include Security Classification) Prediction of Propeller Blade Pressure Distribution with a Panel Method	
12. PERSONAL AUTHOR(S) Yang, Cheng-I	
13a. TYPE OF REPORT Final 13b. TIME COVERED FROM_____TO_____	14. DATE OF REPORT (YEAR, MONTH, DAY) 1990 May 15. PAGE COUNT 47
16. SUPPLEMENTARY NOTATION	
17. COSATI CODES FIELD / GROUP / SUB-GROUP	18. SUBJECT TERMS (Continue on reverse if necessary and identify by block number)

19. ABSTRACT (Continue on reverse if necessary and identify by block number)

Panel methods and their underlying theory are reviewed with regard to hydrodynamic analysis of propeller performance. Green's identity is used to convert the differential Laplace's equation into an integral equation. The velocity potential on the surface of the lifting body can be expressed by integrating the potential induced by source/doublet singularities distributed over the surface. The numerical discretizations of the boundary surface, singularity distributions, the integral equation, and the formulation of the panel method are discussed. The advantages of the application of panel methods in viscous/inviscid interactive procedures and propeller blade design are outlined. Results of propeller blade analysis with the panel method are presented, comparing the prediction of the VSAERO panel method and a vortex lattice method with experimental data. The panel method, which includes consideration of propeller hub effects, gives predictions in good agreement with experimental data.

20. DISTRIBUTION/AVAILABILITY OF ABSTRACT ☒ UNCLASSIFIED/UNLIMITED ☐ SAME AS RPT ☐ DTIC USERS	21. ABSTRACT SECURITY CLASSIFICATION Unclassified
22a. NAME OF RESPONSIBLE INDIVIDUAL Cheng-I Yang	22b. TELEPHONE (Include Area Code) (301) 227-5080 22c. OFFICE SYMBOL Code 1544

CONTENTS

FIGURES

FIGURES (Continued)

NOMENCLATURE

[A]	Influence coefficient matrix (dimension N by N) (Eq. 36)
B	Boundary condition vector (dimension N) (Eq. 36)
B_{ij}	Surface integration of the kernel K_1 over panel containing collocation point i with respect to collocation point j, or induced velocity potential at collocation point j due to doublet distributed on surface panel containing collocation point i (Eq. 35)
C_{ij}	Surface integration of the kernel K_2 over panel containing collocation point i with respect to collocation point j, or induced velocity potential at collocation point j due to doublet distributed on surface panel containing collocation point i (Eq. 35)
C_p	Local pressure coefficient, $(p-p_\infty)/(1/2\ \varrho\ V_R^2)$
D	Propeller diameter
E_c	Meanline ordinate of blade section (Table 1)
E_T	Half thickness ordinate of blade section (Table 1)
f, g	Scalar fields possessing continuous second derivatives (Eq. 2)
f_m	Camber of section (Table 1)
i,j	Subscript used to denote quantities associated with the *i*-th, *j*-th control point (Eq. 34)
ij	Double subscript used to denote effect of *j*-th panel at i-th control point (Eq. 35)
i_G	Blade rake (Table 1)
J	Advance coefficient, $J = V_A/nD$ (Table 1)
K_1,K_2	Scalar kernel functions (Eq. 24)
K_3,K_4	Vector kernel functions (Eq. 21)
K_Q	Torque coefficient, $K_Q = Q/\varrho n^2D^5$
K_T	Thrust coefficient, $K_T = T/\varrho n^2D^4$
l	Section chordlength

NOMENCLATURE (Continued)

M	Total number of surface panels used to approximate the wake surface (Eq. 34)
N	Total number of surface panels used to approximate the body surface (Eq. 34)
$\vec{n}$	Unit normal vector on S, positive pointing into Ω
n	Propeller revolutions per unit time
P	A fixed point interior to the domain Ω; also propeller section pitch or total pressure at local position of blade
Q	A source point interior of the domain Ω, or Propeller torque
$\vec{R}$	Position vector of a field point on propeller blade surface
r	Length of a vector $\vec{r}$ from point Q to P; also radial distance
S, S′	Surface boundary associated with Ω, Ω' (Eq. 4)
T	Propeller thrust
t	Thickness of section
V	Water speed in tunnel test section
V_A	Speed of advance of propeller
V_n	Velocity component normal to surface (Eq. 29)
V_R	Resultant inflow to blade section, $[V^2+(2\pi nr)]^{1/2}$
$\vec{V}_s(P)$, $\vec{V}_d(P)$	Induced velocity vector at point P due to source strength σ, and due to doublet strength μ located at Q, respectively (Eq. 22)
w	subscript used to denote quantities associated with wake (Eq. 24)
x, y, z	Coordinates of a point in the reference coordinate system
x_c	Fraction of chord from leading edge
x_R	Fraction of propeller radius
∞	Subscript used to denote quantities associated with the on set flow

NOMENCLATURE (Continued)

ε	Radius of the sphere surrounding a singular point (Eq. 5a)
θ	Propeller section skew angle
μ	Surface doublet density (Eq. 23)
ϱ	Density of water
σ	Surface source density (Eq. 22)
Φ	Velocity potential (Eq. 3)
Φ_s, Φ_d	Induced velocity potential at point P from a σ, μ located at Q (Eq. 23)
Ω, Ω'	Domain of integration (Eq. 4)
ω	Angular velocity of propeller blade (Eq. 31)
∇	Vector gradient operator
∇_P, ∇_Q	Vector gradient operator taken with respect to coordinate points P and Q, respectively (Eq. 23)

THIS PAGE INTENTIONALLY LEFT BLANK

ABSTRACT

Panel methods and their underlying theory are reviewed with regard to hydrodynamic analysis of propeller performance. Green's identity is used to convert the differential Laplace's equation into an integral equation. The velocity potential on the surface of the lifting body can be expressed by integrating the potential induced by source/doublet singularities distributed over the surface. The numerical discretizations of the boundary surface, singularity distributions, the integral equation, and the formulation of the panel method are discussed. The advantages of the application of panel methods in viscous/inviscid interactive procedure and propeller blade design are outlined. Results of propeller blade analysis with the panel method are presented, comparing the predictions of the VSAERO panel method and a vortex lattice method with experimental data. The panel method, which includes consideration of propeller hub effects, gives predictions in good agreement with experimental data.

ADMINISTRATIVE INFORMATION

This investigation was sponsored by the Chief of Naval Research, Office of Naval Technology (Code OCNR23) under the Ship and Submarine Technology Program, Program Element 62543N, ONT thrust area RS43-434 Propeller Quieting. The work was performed at the David Taylor Research Center under Work Unit 1508-001.

INTRODUCTION

Laplace's equation is one of the most frequently encountered equations in the field of engineering. It governs the potential of an electrostatic field, the stress function of torsion, and the potential of an incompressible inviscid irrotational flow field. The methods of solution have been known for quite some time and can be formulated in either differential or integral forms. The exact solutions can be found for a number of problems with simplified geometries. The problem of interest – marine propeller hydrodynamics – involves extremely complicated geometries, and solutions can be obtained only numerically. The availability of modern high-speed computing machinery and the maturity of some numerical techniques have resulted in the recent development of panel methods.[1-5]

The panel method has a distinct advantage over the differential approaches, such as finite-element or finite-difference methods, because the unknowns of the panel method are situated only on the fluid/solid interface and not throughout the external space. In principle, the method applies only to incompressible, inviscid, and irrotational flow. However, due to recent developments of inviscid/viscid interactive techniques, the application can be extended to problems with mild boundary layer separation and cavitation. In the propeller hydrodynamics application, when the geometry of a given propeller blade and its

advance coefficient are specified, the panel method is capable of calculating the pressure, lift, drag, and moment on blades,[6] duct, or band. With the implementation of a wake relaxation procedure, the wake contraction can also be predicted.[5] If the total number of unknowns can be kept to a tolerable level, the panel method can also be applied to the problems of propeller/rudder and propeller/hull interactions.

In the propeller hydrodynamics application, as reported[6] earlier, the panel method is capable of providing reliable surface pressure distributions in the blade leading-edge region. It was also shown that the method is capable of predicting the leading-edge pressure peak when the propeller is operating at off-design advance ratio, although comparison with experimental data is insufficient. The purpose of this report is to reinforce Hess's observations through comparison of various solutions obtained by the panel method, the lifting surface theory, the equivalent two-dimensional theory, and extensive experimental data acquired at the David Taylor Research Center (DTRC). Some details of the panel method formulation are outlined.

MATHEMATICAL BACKGROUND

GOVERNING EQUATIONS

For steady, inviscid, irrotational, and incompressible flows in the domain Ω bounded by the surface S, there exists a velocity potential that satisfies the Laplace's equation, with appropriate boundary conditions at S,

$$\nabla^2 \Phi = 0 \tag{1}$$

where

$$\nabla^2 = \frac{\partial^2}{\partial x^2} + \frac{\partial^2}{\partial y^2} + \frac{\partial^2}{\partial z^2}$$

and x, y, and z are the orthogonal coordinate axes. The assumptions made in deriving Eq. 1 and the consequence of the assumptions are described in the Appendix.

BOUNDARY CONDITIONS

Two types of boundary conditions are often found in hydrodynamic applications: (a) the Neuman-type boundary condition (specifying the derivative of the potential Φ) applied at the Kutta point or on the wetted surface and (b) the Dirichlet-type boundary condition (specifying the potential) applied at the internal flow to render a unique solution of external flow problems via Green's third identity. The Dirichlet-type boundary condition may also arise in design procedures in which the surface pressure distribution is specified.

The idealized flow and its boundaries can be represented as shown in Fig. 1. On the solid surface, the velocity component normal to the surface is set to zero for a nonpermeable condition, or to the boundary layer transpiration velocity if inviscid/viscid interaction is implemented. Wakes that carry away the

vorticity generated in the boundary layer on the body may be assumed to attach to the sharp edges, such as the trailing edge, leading edge, tip, or a line of separation. Suppose in Fig. 1 that the potential is Φ_1 in the external region Φ_1, Φ_2 in the internal region Ω_2, and Φ_3 in the wake region Ω_3. The potentials Φ_2 and Φ_3 do not simulate the real flow; only their influences on the external region are simulated.

INTEGRAL EQUATIONS

Suppose a domain Ω is bounded by a surface S as shown in Fig. 2. If f and g are any two similar fields which possess continuous second derivatives, then Green's identity states

$$\int_{\Omega} (g\nabla^2 f - f\nabla^2 g)d\Omega = \int_S (f\vec{n}\cdot\nabla g - g\vec{n}\cdot\nabla f)dS \tag{2}$$

with the unit vector $\vec{n}$ normal to the surface S and pointing into the domain Ω. Suppose g is replaced by a velocity potential Φ that satisfies Laplace's equation $\nabla^2\Phi = 0$ and f is replaced by $1/r$, where r is the length of a vector $\vec{r}$ from any source point Q interior to the domain Ω to a fixed point P. The function $1/r$ possesses second-order derivatives and satifies Laplace's equation $\nabla^2(1/r) = 0$ at all P, except when P is interior to Ω or on S.

When P is exterior to Ω, straightforward application of Eq. 2 results in

$$\int_S [1/r\ \vec{n}\cdot\nabla\Phi - \Phi\vec{n}\cdot\nabla(1/r)]dS = 0. \tag{3}$$

When P is interior to Ω, $1/r$ becomes singular as Q approaches P. The singularity can be avoided by surrounding the fixed point P with a small sphere of radius ε, surface S', and volume Ω', and applying Eq. 2 to the volume $\Omega - \Omega'$ and surface $S + S'$, to obtain

$$\int_{S+S'} [(1/r)\ \vec{n}\cdot\nabla\Phi - \Phi\vec{n}\cdot\nabla(1/r)]dS = 0. \tag{4}$$

As the radius ε of the sphere surrounding P approaches zero, the following limits can be obtained:

$$\int_{S'} (1/\varepsilon)\ \vec{n}\cdot\nabla\phi\ dS' \to 0 \tag{5a}$$

and

$$\int_{S'} \Phi\vec{n}\cdot\nabla\ (1/r)\ dS' \to -4\pi\Phi(P). \tag{5b}$$

Equations 4 and 5 imply

$$4\pi\Phi(P) = \int_S [\Phi\vec{n}\cdot\nabla\ (1/r) - 1/r\ \vec{n}\cdot\nabla\Phi]dS. \tag{6}$$

When P lies on the surface S, 1/r becomes singular as Q approaches P. The singularity can be avoided in a manner similar to that just described. If the surface S is smooth (first-order derivatives are continuous), the following limits can be obtained:

$$\int_{S'} (1/\varepsilon)\, \vec{n}\cdot\nabla\Phi \, dS' \to 0 \tag{7a}$$

and

$$\int_{S'} \Phi\vec{n}\cdot\nabla(1/r)\, dS' \to -2\pi\Phi(P). \tag{7b}$$

It is concluded that

$$\int_S (\Phi\vec{n}\cdot\nabla\,(1/r) - 1/r\,\vec{n}\cdot\nabla\Phi)\, dS = \begin{cases} 0: & P \text{ lies exterior of } \Omega \\ 4\pi\Phi(P): & P \text{ lies interior of } \Omega \\ 2\pi\Phi(P): & P \text{ lies on S.} \end{cases} \tag{8}$$

The function f in Eq. 2 was introduced by Green in solving Laplace's equation $\nabla^2 g = 0$ and was called Green's function later by Riemann. It is clear from Eq. 8 that with the help of Green's function the potential at any fixed point P can be expressed in terms of its value on the surface. Such a method of solving Laplace's equation, as opposed to the method of using series of special functions, is called the method of singularities.

The geometry of practical problems is complicated and often involves multiple domains. Figure 1 represents the geometry of a lifting body problem. It involves three distinct domains, Ω_1, Ω_2 and Ω_3. The domain Ω_1 is the external flow field, Ω_2 is the lifting body separated from Ω_1 by the boundary surface S_{12}, and Ω_3 is the wake separated from Ω_1 by the surface S_{13} and from Ω^2 by the surface S_{23}. As mentioned previously, the potentials Φ_2 and Φ_3 in Ω_2 and Ω_3 are used to simulate effects on the external flow field Ω_1 and not the real flow of a lifting body or wake.

Consider a fixed point P lying in the external flow field Ω_1 and apply Eq. 8 in terms of the potential Φ_1:

$$\begin{aligned} 4\pi\Phi(P) = &\int_{S_{12}} - (1/r)\,\vec{n}_1\cdot\nabla\Phi_1\, dS + \int_{S_{12}} \Phi_1\vec{n}_1\cdot\nabla(1/r)\, dS \\ &+ \int_{S_{13}} - (1/r)\,\vec{n}_1\cdot\nabla\Phi_1\, dS + \int_{S_{13}} \Phi_1\vec{n}_1\cdot\nabla(1/r)\, dS \\ &+ \int_{S_0} - (1/r)\,\vec{n}_1\cdot\nabla\Phi_1\, dS + \int_{S_0} \Phi_1\vec{n}_1\cdot\nabla(1/r)\, dS \end{aligned} \tag{9}$$

Since P lies in Ω_1 and is outside of Ω_2, and since, $\vec{n}_2 = -\vec{n}_1$ on S_{12}, Eq. 8 applied in terms of the potential Φ_2 gives

$$0 = -\int_{S_{12}} -(1/r)\,\vec{n}_1\cdot\nabla\Phi_2\,dS + \int_{S_{12}} -\Phi_2\vec{n}_1\cdot\nabla(1/r)\,dS$$
$$+\int_{S_{23}} -(1/r)\,\vec{n}_2\cdot\nabla\Phi_2\,dS + \int_{S_{23}} \Phi_2\vec{n}_2\cdot\nabla(1/r)\,dS. \qquad (10)$$

Since P is outside of Ω_3 and $\vec{n}_3 = -\vec{n}_1$ on S_{13}, if we apply Eq. 8 in terms of the potential Φ_3 we have

$$0 = -\int_{S_{13}} -(1/r)\,\vec{n}_1\cdot\nabla\Phi_3\,dS + \int_{S_{13}} -\Phi_3\vec{n}_1\cdot\nabla(1/r)\,dS$$
$$+\int_{S_{23}} -(1/r)\,\vec{n}_3\cdot\nabla\Phi_3\,dS + \int_{S_{23}} \Phi_3\vec{n}_3\cdot\nabla(1/r)\,dS. \qquad (11)$$

Summing the contribution of all surfaces to the potential at point P, we have

$$4\pi\Phi(P) = \int_{S_{12}} -(1/r)\,\vec{n}_1\cdot(\nabla\Phi_1-\nabla\Phi_2)\,dS + \int_{S_{12}} (\Phi_1-\Phi_2)\,\vec{n}_1\cdot\nabla(1/r)\,dS$$
$$+\int_{S_{13}} -(1/r)\,\vec{n}_1\cdot(\nabla\Phi_1-\nabla\Phi_3)\,dS + \int_{S_{13}} (\Phi_1-\Phi_3)\,\vec{n}_1\cdot\nabla(1/r)\,dS$$
$$+\int_{S_{23}} -(1/r)\,\vec{n}_2\cdot(\nabla\Phi_2-\nabla\Phi_3)\,dS + \int_{S_{23}} (\Phi_2-\Phi_3)\,\vec{n}_2\cdot\nabla(1/r)\,dS$$
$$+\int_{S_0} -(1/r)\,\vec{n}_1\cdot\nabla\Phi_1\,dS + \int_{S_0} \Phi_1\,\vec{n}_1\cdot\nabla(1/r)\,dS. \qquad (12)$$

If the outer surface S_0 lies infinitely far away from the other surfaces and the point P lies near S_0, the contributions of surfaces S_{12}, S_{13}, and S_{23} to the point P become negligible and Eq. 12 becomes

$$4\pi\Phi_\infty = \int_{S_0\to\infty} -(1/r)\,\vec{n}_1\cdot\nabla\Phi_1\,dS + \int_{S_0\to\infty} \Phi_1\vec{n}_1\cdot\nabla(1/r)\,dS \qquad (13)$$

where Φ_∞ represents the unperturbed potential in the far field. If the wake is assumed to be infinitely thin, the surface length S_{23} approaches zero and its contribution to the potential at point P vanishes. The wake effect on the potential at point P is represented by the surface integral on S_{13} in Eq. 12:

$$\int_{S_{13}} -(1/r)\,\vec{n}_1\cdot(\nabla\Phi_1-\nabla\Phi_3)\,dS + \int_{S_{13}} (\Phi_1-\Phi_3)\,\vec{n}_1\cdot\nabla(1/r)\,dS. \qquad (14)$$

Expression 14 can be decomposed to upper (+) and lower(−) surfaces:

$$\int_{S_{13}^+} (1/r)\,\vec{n}^+ \cdot (\nabla\Phi_1^+ - \nabla\Phi_3^+)\,dS + \int_{S_{13}^+} (\Phi_1^+ - \Phi_3^+)\,\vec{n}^+ \cdot \nabla\,(1/r)\,dS$$

$$+ \int_{S_{13}^-} (1/r)\,\vec{n}^- \cdot (\nabla\Phi_1^- - \nabla\Phi_3^-)\,dS + \int_{S_{13}^-} (\Phi_1^- - \Phi_3^-)\,\vec{n}^- \cdot \nabla\,(1/r)\,dS. \quad (15)$$

In the limit of infinitesimal wake thickness, the following situations arise:

$$\vec{n}^+ = -\vec{n}^-$$

and

$$\Phi_3^+ = \Phi_3^-.$$

Equation 15 then becomes

$$\int_{S_{13}} (1/r)\,\vec{n}^+ \cdot (\nabla\Phi_1^+ - \nabla_1\Phi^-)\,dS^+ + \int_{S_{13}} (\Phi_1^+ - \Phi_1^-)\,\vec{n}^+ \cdot \nabla\,(1/r)\,dS. \quad (16)$$

If the wakes are assumed to be nonload-carrying with no flow entrainment, then the potential gradient across the wake surface is continuous and the first term in Eq. 16 vanishes. The potential jump across the wake surface in the second term in Eq. 16 can be replaced by $\Delta\Phi$ and Eq. 12 can then be written as

$$4\pi\Phi(P) = \int_{S_{12}} -(1/r)\,\vec{n}_1 \cdot (\nabla\Phi_1 - \nabla\Phi_2)\,dS + \int_{S_{12}} (\Phi_1 - \Phi_2)\,\vec{n}_1 \cdot \nabla\,(1/r)\,dS$$

$$+ \int_{S_{13}} \Delta\Phi\vec{n}_1 \cdot \nabla\,(1/r)\,dS + 4\pi\Phi_\infty. \quad (17)$$

If P is on the surface of S_{12}, the potential at P can be derived in a similar manner by repeated application of Eq. 8; this gives

$$2\pi\Phi_1(P) + 2\pi\Phi_2(P) = \int_{S_{12}} -(1/r)\,\vec{n}_1 \cdot (\nabla\Phi_1 - \nabla\Phi_2)\,dS + \int_{S_{12}} \vec{n}_1 \cdot \nabla\,(1/r)\,(\Phi_1 - \Phi_2)\,dS$$

$$+ \int_{S_{13}} \Delta\Phi\vec{n}_1 \cdot \nabla\,(1/r)\,dS + 4\pi\Phi_\infty \quad (18)$$

where $\Phi_1(P)$ and $\Phi_2(P)$ are the potentials at point P on the external and internal sides of Ω_2 of the surface S_{12}, respectively. Equation 18 can be rewritten in the following two forms:

$$4\pi\Phi_1(P) = \int_{S_{12}} -(1/r)\,\vec{n}_1 \cdot (\nabla\Phi_1 - \nabla\Phi_2)\,dS + \int_{S_{12}} \vec{n}_1 \cdot \nabla\,(1/r)\,(\Phi_1 - \Phi_2)\,dS$$

$$+ \int_{S_{13}} \Delta\Phi\vec{n}_1 \cdot \nabla\,(1/r)\,dS + 4\pi\Phi_\infty + 2\pi\,[\Phi_1(P) - \Phi_2(P)], \quad (19)$$

and

$$4\pi\Phi_2(P) = \int_{S_{12}} - (1/r)\,\vec{n}_1\cdot(\nabla\Phi_1 - \nabla\Phi_2)\,dS + \int_{S_{12}} \vec{n}_1\cdot\nabla\,(1/r)\,(\Phi_1 - \Phi_2)\,dS$$
$$+ \int_{S_{13}} \Delta\Phi\vec{n}_1\cdot\nabla\,(1/r)\,dS + 4\pi\Phi_\infty - 2\pi\,[\Phi_1(P) - \Phi_2(P)]. \qquad (20)$$

The velocity at point P can be obtained by applying the ∇_P operator (the derivatives being evaluated with respect to the coordinates of point P) to Eqs. 17, 19, or 20, depending on the location of point P. For illustrative purposes, the application of the ∇_P operator is as follows:

$$4\pi\nabla_P\Phi_1(P) = \int_{S_{12}} \vec{K}_3\,(\nabla\Phi_1 - \nabla\Phi_2)\,dS + \int_{S_{12}} \vec{K}_4\,(\Phi_1 - \Phi_2)\,dS$$
$$+ \int_{S_{13}} \vec{K}_4\,\Delta\Phi\,dS + 4\pi V_\infty + 2\pi\,[\nabla_P\Phi_1(P) - \nabla_P\Phi_2(P)]$$
$$= 4\pi\vec{V}(P) \qquad (21)$$

where $\vec{K}_3$ [$= -\nabla_P(1/r) = \vec{r}/r^3$] and $\vec{K}_4$ [$= \nabla_P[\vec{n}_1\cdot\nabla(1/r)] = (\vec{n}_1\cdot\nabla_P)\,\vec{r}/r^3$] are vector kernel functions which depend only on the geometry and are independent of flow or boundary conditions.

As a consequence of Green's identity, Eq. 19 and Eq. 21 show that $\Phi_1(P)$ and $V_1(P)$, the potential and velocity of a field point P in the external region Ω or on the external surface of S_{12}, can be expressed in terms of the distribution of $\vec{n}_1\cdot(\nabla\Phi_1 - \nabla\Phi_2)$, $(\Phi_1 - \Phi_2)$ on S_{12}, and $\Delta\Phi$ on the surface of the wake. The value $\Phi_1(P)$ or $\vec{V}_1(P)$ can be uniquely determined on " if boundary conditions for Φ_2 on the internal flow region Ω_2 are specified. The boundary conditions for Φ_2 depend on the physical problems encountered. They may also affect the numerical error and stability of the solution of $\Phi_1(P)$ and $V_1(P)$.

A point source of strength σ at source point Q induces a potential $\Phi_s(P)$ and velocity $V_s(P)$ at a point P[7] such that

$$\Phi_s(P) = -\frac{\sigma}{4\pi r}$$

and

$$\vec{V}_s(P) = \frac{\sigma}{4\pi}\frac{\vec{r}}{r^3} \qquad (22)$$

where r is the magnitude of the vector $\vec{r}$ pointing from Q to P. A doublet of strength μ at source point Q induces a potential $\Phi_d(P)$ and velocity $\vec{V}_d(P)$ at point P such that

$$\Phi_d(P) = -\frac{1}{4\pi}\mu\vec{n}\cdot\nabla_Q(1/r) = \frac{1}{4\pi}\mu\vec{n}\cdot\nabla_P(1/r)$$

and

$$\vec{V}_d(P) = \frac{1}{4\pi}\mu\,\nabla_P[\vec{n}\cdot\nabla_P\,(1/r)] \tag{23}$$

where $\vec{n}$ is the normal along the axis of the doublet pointing from the negative to the positive end of the doublet. The derivatives in the vector operator ∇_P and ∇_Q are taken with respect to the coordinates of points P and Q, respectively.

With Eq. 22, the first integral on the right-hand side of Eq. 19 can be interpreted as the potential induced at point P due to a source distribution on surface S_{12} whose strength is equal to the boundary value of $\vec{n}_1\cdot(\nabla\Phi_1 - \nabla\Phi_2)$. With Eq. 23, the second integral of the same equation can be interpreted as the potential induced at point P due to a distribution of doublets on S_{12} whose axes lie along with the unit normal surface vector n_1 and whose strength is the boundary value of $-(\Phi_1 - \Phi_2)$. Note that the derivatives of the vector operator Δ in this integral are taken with respect to the coordinates of source point Q on surface S_{12}. Equation 19 can now be written as

$$4\pi\Phi_1(P) = \int_{S_{12}}(K_1\sigma - K_2\mu)\,dS + \int_{S_{13}}\mu_w K_2\,dS + 4\pi\Phi_\infty - 2\pi\mu(P) \tag{24}$$

where K_1 [$= -(1/r)$] and K_2 [$= \vec{n}_1\cdot\nabla_P(1/r) = \vec{n}_1\cdot\vec{r}/r^3$] are scalar kernel functions which depend only on the geometry of the boundary and wake shape and are independent of the flow and boundary conditions, and μ_w is the doublet strength at the wake surface to be determined from a Kutta condition. Likewise, Eq. 21 can be written as

$$4\pi\vec{V}(P) = \int_{S_{12}}\vec{K}_3\sigma\,dS - \int_{S_{12}}\vec{K}_4\mu\,dS + \int_{S_{13}}\vec{K}_4\mu_w\,dS + 4\pi\vec{V}_\infty + 2\pi\sigma(P)n_1 \tag{25}$$

where $\vec{n}_1$ is the outward normal at point P.

The concept of placing singularities such as sources and doublets of specified strength over the boundary surfaces of a flow field forms the basis of the surface singularity technique. As discussed previously, various assumptions and boundary conditions regarding the internal field may be used to obtain a unique solution for problems which are physically meaningful. Different assumptions demand different solution techniques. The choice of assumption depends on the nature of the problem, such as lifting or nonlifting bodies, thick or thin wing sections, etc. If the integral equations are to be solved numerically, the assumptions play an important role in the errors and accuracy of the solutions. Some interesting and practical formulations are given in the following sections.

SOURCE-ONLY FORMULATION

This formulation was adopted by Hess and Smith[2] to solve the potential flow about arbitrary nonlifting bodies. The internal potential Φ_2 is assumed to be continuous, and at the wetted surface it has the same value as the external total potential ($\Phi_1 - \Phi_2 = 0$ at S_{12} in Fig. 1). The normal derivative of Φ is discontinuous at the surface. After the inner product of Eq. 25 and the normal vector n_1 at point P has been taken and the terms grouped, Eq. 25 becomes

$$2\pi\sigma(P) + \int_{S_{12}} (\vec{K}_3 \cdot \vec{n}_1)\sigma \, dS = -4\pi (\vec{V}_\infty - \vec{V}(P)) \cdot \vec{n}_1. \tag{26}$$

Equation 26 is an integral equation since the unknown source strength σ appears under an integral sign. The equation is identified as the Fredholm integral equation of the second kind. Numerical discretization converts the integral equation into a system of linear equations denoted by

$$[A]\sigma = b$$

where [A] is the influence coefficient matrix, and b is the boundary condition, σ is to be solved at the discretized points. With the presence of the singular term $2\pi\sigma(P)$ in Eq. 26, [A] becomes diagonal dominating and well conditioned.

DOUBLET-ONLY FORMULATION

The normal gradients of Φ_1 and Φ_2 are assumed to be equal at the wetted surface, separating the region Ω_1 from the region Ω_2 ($\vec{n} \cdot (\nabla\Phi_1 - \nabla\Phi_2) = 0$ at S_{12}). After implementation of this assumption, the σ terms vanish from Eqs. 24 and 25. This leads to the doublet-only formulation. Physically, this assumption implies that the normal component of the velocity at the inner and outer surfaces of the wetted surface S_{12} is continuous. If the wetted surface is solid, then $V_n = 0$ at the inner surface and Φ_2 becomes constant everywhere in Ω_2. After the σ term has been dropped and the inner product with the normal vector $\vec{n}_1$ taken, Eq. 25 becomes

$$4\pi\vec{V}(P) \cdot \vec{n}_1 = 4\pi\vec{V}_\infty \cdot n_1 - \int_{S_{12}} \mu(\vec{K}_4 \cdot \vec{n}_1) \, dS + \int_{S_{13}} \mu_w(\vec{K}_4 \cdot \vec{n}_1) \, dS. \tag{27}$$

Equation 27 is a Fredholm integral equation of the first kind with μ to be solved. Through numerical discretization, Eq. 27 can be converted to a system of linear equations $[A]\mu = b$ where [A] is singular; that is, the sum of the elements in every row is zero. The system of equations is not linearly independent. To obtain a unique solution, an additional condition is required. One of the conditions is to specify a fixed value of μ at a given point on S_{12}.

SOURCE AND DOUBLET FORMULATION

Equation 20 expresses the potential at point P on surface S_{12} on the Ω_2 side and can be rewritten in terms of source and doublet distributions as

$$4\pi\Phi_2(P) = \int_{S_{12}} (K_1\sigma_1 - K_2\mu)\, dS + \int_{S_{13}} \mu_w K_2\, dS + 2\pi\mu(P) + 4\pi\Phi_\infty \qquad (28)$$

where K_1 and K_2 are the scalar kernel functions as defined in Eq. 24. The obvious external boundary condition on the wetted surface is

$$\vec{n}_1 \cdot \nabla\Phi_1 = V_n. \qquad (29)$$

V_n is zero if the surface is solid. As mentioned earlier, to obtain a unique solution of Eq. 28, some assumption regarding the internal flow field should be made. Johnson,[8] Bristow,[9] and Maskew[5, 10] have applied a Dirichlet condition to the internal flow field and set $\Phi_2 = \Phi_\infty$. With these defined internal and external boundary conditions, the source strength on the surface can be written

$$\sigma = \vec{n}_1 \cdot (\nabla\Phi_1 - \nabla\Phi_2) = V_n - \vec{n}_1 \cdot \vec{V}_\infty. \qquad (30)$$

Suppose the lifting body under consideration is a propeller blade which rotates about an axis with angular velocity ω. The analysis derived previously still holds with respect to a moving frame fixed to the propeller blade. In this moving frame fixed to the propeller, the boundary condition expressed in Eq. 29 becomes

$$\vec{n}_1 \cdot \nabla\Phi_1 = V_n - \vec{n}_1 \cdot \vec{\omega} \times \vec{R} \qquad (31)$$

where R is the position vector of point P on the surface of the propeller with respect to the frame fixed to the propeller. Equation 30 becomes

$$\sigma = \vec{n}_1 \cdot (\nabla\Phi_1 - \nabla\Phi_2) = V_n - \vec{n}_1 \cdot \vec{V}_\infty - \vec{n}_1 \cdot \omega \times \vec{R}. \qquad (32)$$

All quantities on the right-hand side of Eq. 32 are known. It is now clear that application of the Dirichlet boundary condition on the internal region determines the source strength σ in Eq. 28. Equation 28 can be written as

$$2\pi\mu(P) = -\int_{S_{12}} K_1\sigma\, dS - \int_{S_{13}} K_2\mu_w\, dS + \int_{S_{12}} K_2\mu(Q)\, dS \qquad (33)$$

and Q is a source point on surface S_{12} excluding P. Equation 28 is a Fredholm integral equation of the second kind and can be solved uniquely in terms of the doublet strength μ.

SOURCE AND VORTICITY FORMULATION

A constant-strength doublet panel is equivalent to a ring of line vortices around the perimeter. Hess[11] proved in a more general case that a surface doublet distribution of density μ can be replaced by a vortex sheet (on the same surface as the doublet sheet) plus a concentrated vortex filament around the edge of the sheet. The vorticity $\vec{\gamma}$ on the sheet can be related to the doublet as

$$\gamma = \vec{n} \times \nabla\mu$$

where $\vec{n}$ is the unit normal vector of the surface and $\nabla\mu$ is the gradient of the doublet strength. The strength of the concentrated vortex filament around the edge is equal to the local edge doublet strength.

In the three-dimensional case, the magnitude of the strength and the direction of the vortex are unknown. Care must be taken to ensure that Kelvin's circulation condition (zero divergence) is satisfied everywhere. The numerical implementation of the vorticity formulation is more complicated than for the source/doublet formulation. Bristow[9] preferred the source/doublet formulation over the source/vorticity formulation for the design problem.

Although all types of singularity distributions just discussed can be derived directly or indirectly from Green's identity, the resulting numerical formulations and accuracies are quite different. Bristow[9] showed that the source/doublet distribution in general provides a source distribution milder than the source-only solution and a doublet distribution milder than the doublet-only distribution. In summary, the source/doublet distribution is attractive because

1. Relatively mild singularity distributions suppress the numerical instabilities, which may otherwise be prevalent for these high lift geometries.

2. Direct relationships between velocity and singularity strengths on the boundary surface simplify calculations; which facilitates implementation of the boundary layer displacement formulation for inviscid/viscous interaction.

3. Singularity distributions vanish as the perturbation field vanishes, thereby eliminating possible residual errors.

4. With a source/doublet distribution, it is easier to obtain a numerically stable solution in the design problem.

NUMERICAL DISCRETIZATION

The conversion of a differential equation to an integral equation, illustrated in a previous section, becomes a major technique for solving initial-value and boundary-value problems of ordinary and partial differential equations. Only in a limited number of cases can the Fredholm equation be solved in closed analytical forms. In general, these equations must be solved numerically. The Fredholm integral equation of the first kind is more difficult to solve than the second kind. For this reason, the discretization of Eq. 33 with appropriate boundary conditions will be addressed here. The complete discretization of the problem involves three different tasks; (a) discretization of the boundary condition, (b) discretization of surface geometry, and (c) discretization of the singularity distribution.

DISCRETIZATION OF THE BOUNDARY CONDITION

A continuous solution of an integral equation demands that the boundary condition be satisfied on the physical boundary in a continuous manner. With a numerical approach, the boundary condition can be satisfied only at a finite number of selective collocation points. Consequently, the velocity components and potential at the physical surface between the collocation points are not

likely to satisfy the imposed condition. For example, if the normal component V_n of the velocity is prescribed at the boundary, the discretized solution will give the potential field that produces the correct velocity component only at the discretized collocation points on the boundary. Between the collocation points, the calculated potential field in general will give a value for V_n that is quite different from the physical one. This difference is sometimes referred to as leakage. The problem is inherent in discretization. The leakage may not be eliminated completely but can be reduced by using a more accurate surface discretization (more collocation points when the surface normal vector varies rapidly and a smoother distribution of singularity, such as provided by a higher order model).

DISCRETIZATION OF THE GEOMETRICAL SURFACE

The smooth continuous shape of the body surface is represented by a number of plane quadrilateral panels whose corners are the projection of the surface points on the panels. Use of a flat panel to approximate a curved surface, makes it inevitable that geometrical discontinuities will exist on the surface of the panels where the singularities are distributed. To approximate the continuous physical surface meaningfully with a collection of flat panels, the deviations of the surface points and their projection on the panel plane should be kept as small as possible. On a surface area where curvature is large, small panels should be used. The centroid of the panel plane can be taken as the collocation point on which the boundary conditions are applied.

The collocation point on the centroid of the plane panel may not be on the physical surface, and the unit normal vector of the panel may not be aligned with the normal of the physical surface. The deviation between the true and numerical solution depends on the distribution and orientations of the panels. It should be kept in mind that the numerical solution is meaningful only at the collocation points.

DISCRETIZATION OF SINGULARITY DISTRIBUTION

The singularities described previously are distributed on the panel surface rather than on the physical surface. The strengths of the singularities can be constant or can vary continuously over the panel, depending on whether first- or higher order approximations are used. For a simple singularity distribution, the influence of a single panel of arbitrary shape at a given field point can be computed entirely analytically. Some examples can be found in Hess and Smith[1] and Newman.* The discontinuity of the source strength at the edge a of panel may result in an erroneous velocity which becomes logarithmically unbounded in the vicinity of the edge, and the discontinuity of the doublet strength may cause a jump of potential and velocity near the edge. To reduce the error, a consistent higher order approximation is required to provide continuous source and doublet strengths on some points along the edge. The discontinuities of singularity strength may also be eliminated by weighted averaging along a common panel edge. The improved accuracy is obtained at the expense of computational effort. The accuracy of a first-order approximation may be improved by using more panels on surface regions where curvature changes rapidly. The choice of a first- or higher order approximation should be decided by balancing cost and accuracy.

*Newman, J.N., "Distribution of Sources and Normal Dipoles Over a Quadrilateral Panel," *(submitted for publication, 1986).*

NUMERICAL SOLUTION

Numerical discretization and solution of the integral equation, Eq. 33, are discussed here. For illustration purposes, the singularities (source/doublet) are assumed to have constant strength on a given panel. Suppose that the physical surfaces are replaced with N flat panels and the wake surface is replaced with M panels. Equation 33 can then be approximated as

$$2\pi\mu_j = \sum_{\substack{i=1 \\ 1\neq j}}^{N} \int_{S_i} K_2\mu_i \, dS - \sum_{i=1}^{N} \int_{S_i} K_1\sigma_i \, dS - \sum_{i=1}^{M} \int_{S_i} (\mu_w)_i \, K_2 \, dS \quad (34)$$

where μ_i is the doublet strength on the panel, S_i is the area of the panel, and σ_i is the source strength. In the current example, σ is known and assumed to be constant over the panel area S_i. Since the strengths of the singularities are constant on each panel, they can be taken out of the integral signs in Eq. 34. The scale kernel K_1 and K_2 can be integrated over the panel surface analytically.[1,*] Equation 34 can then be written in a simplified form as

$$2\pi\mu_j = \sum_{\substack{i=1 \\ 1\neq j}}^{N} \mu_i C_{ij} - \sum_{i=1}^{N} \sigma_i B_{ij} - \sum_{i=1}^{M} (\mu_w)_i C_{ij} \qquad j = 1, N \quad (35)$$

where B_{ij} and C_{ij} matrices are the surface integration of the kernel K_1 and K_2 over the panel containing field point i with respect to the field point j. Physically, they express the potential induced at collocation point j by the source and doublet distribution on the panel, which contains collocation point i. When the collocation point j is sufficiently far away from point i, the full expression is replaced by a simpler formulation which yields results within a reasonable tolerance.[1] The doublet strength μ_w on the wake surface is determined from a Kutta condition. Equation 35 can be written in matrix form

$$[A]\, X = B \quad (36)$$

where [A] is the influence coefficient matrix which has a dimension of N by N, X is the doublet strength column vector with dimension N, and B is the boundary condition vector with dimension N. The singular term of the Fredholm integral equation of the second kind makes the [A] matrix well conditioned (in general, it is diagonal dominating).

In actual numerical computation, the assembly of the matrix [A] involves the evaluation of B_{ij} and C_{ij} and is very time consuming. [A] is a full matrix, and the solution of Eq. 36 demands also a large amount of computing effort, especially when the number of panels is large. The block Gauss-Seidel method can be used in solving such a large system.

*Newman, J.N., "Distribution of Sources and Normal Dipoles Over a Quadrilateral Panel," (submitted for publication, 1986).

VISCOUS/INVISCID INTERACTION

In virtually every aspect of hydrodynamic problems the viscous effects are significant and must be accounted for. Although the Navier-Stokes equation applies to such flows, it requires significant computational resources[7], especially at high Reynolds number conditions. For this reason, simpler viscous/inviscid interactive approaches were derived.

In a recent review paper on calculation methods for flow on airfoils, Cebeci, Stewartson, and Whitelaw[12] concluded that the interactive approach is more economical than the direct application of Reynolds-averaged two-dimensional forms of the Navier-Stokes equations. In the interactive approach, the flow is divided into an outer inviscid region and a thin viscous region near the solid surface and around the wakes. The inviscid region can be approximated by panel methods if the flow is irrotational. The interaction between inner and outer regions can be established by two different methods. The first method as presented by Mahgoub and Bradshaw,[13] is differential. The regions are matched at an arbitrary line that encloses the solid surface. The inner solution is obtained by finite-differencing the parabolized Navier-Stokes equation, and the outer solution is obtained by the panel method. The second method is integral. In this method, the inner region is not physically prescribed, and the outer region contacts the solid surface directly. The viscous effect is extended to the inviscid region by the deficit formulation, as described by LeBalleur.[14] Both differential and integral methods can able to calculate the flow patterns beyond the separation points with reasonable accuracy. Both methods can be extended to lifting body calculations in which the wake curvature effects are also important. Although the differential method gives more detailed information about the flow field, it is impractical for design purposes because of the huge computational resource required. Kline, Cantwell, and Lilley[15] showed that an integral boundary layer method need not be less accurate than methods based on Reynolds averaged equations.

There are two popular models of the viscous displacement effect in integral methods. One model requires the computation of boundary layer displacement thickness, and the zero-normal-velocity boundary condition is then applied to the modified geometry as described by Dutt and Sreekanth.[16] The other model was originally proposed by Lighthill.[17] It applies a relatively simple transpiration condition on the physical surface. The latter model is more practical if a panel method is being used to compute the inviscid flow, since the matrix of influence coefficients of Eq. 36 need not be computed during the interactive process once it is set up. On the basis of the boundary transpiration concept, Green[18] derived an entrainment method to predict the flow in a turbulent boundary layer. This method has been further improved by East,[19] Lock and Firnin,[20] Le Balleur,[14] and Melnik and Brook[21] to account for flow separation. Other approaches capable of treating flow separation were given by Dvorak, Maskew, and Woodward,[22] Dvorak, Woodward, and Maskew,[23] and Maskew, Rao, and Dvorak.[24] Application of a panel method to attached cavitation has been reported by Franc and Michel.[25]

APPLICATION OF PANEL METHOD AS A DESIGN TOOL

One of the design-type problems involves the determination of body contour that will produce a prescribed pressure distribution. The panel methods have been successful in predicting flow pattern and surface pressure distribution involving complicated geometries in potential flow, but they are not widely used in designing lifting-surface elements. One of the reasons is that the design problem is more complicated than the analysis problem, and the design formulation is often unstable unless some precautions are taken. The other reason is that, due to the non-linearity of the boundary conditions, an iterative approach is needed to obtain a solution and the computing cost becomes prohibitive. Several design methods based on the panel approach have been reported in the past for designing wing section contours that will produce a prescribed pressure distribution,[26,27] but not all are satisfactory. Some of the drawbacks are (a) the calculations fail to coverage, (b) the design contour is unrealistically wavy, and (c) computing cost is prohibitive. Slooff[28] has discussed several other design methods.

Bristow[29] and Hawk[30] developed a perturbation analysis/design method for analyzing a series of arbitrary small-geometry perturbations to a baseline configuration and for designing a wing section that will produce a prescribed pressure distribution. The method is based on the panel method with source/doublet surface singularity distributions described previously (constant source and quadratic doublet distribution). The authors reported that the method is cost effective, accurate, and stable.

The perturbation analysis method was developed for efficient and accurate analysis of a series of arbitrary small geometry perturbations to a baseline configuration. The velocity potential for the perturbed configuration is obtained by a first-order Taylor series expansion about the velocity potential of the baseline configuration. Basically, it is a linear extrapolation procedure and bypasses the two most expensive steps: (a) assembling the new influence coefficient matrix, and (b) solving a large system of linear algebraic equations for the velocity potential. The authors attributed the success of the method to the fact that only the velocity potential—not velocity and pressure—is linearized with respect to the geometry perturbation coordinate, and the nonlinear terms are much smaller for velocity potential than for either velocity or pressure. The method is applicable to large perturbations of wing thickness, camber, and twist.

The perturbation design method is the logical extension of the perturbation analysis method already described. The design can be initiated from a baseline geometry obtained from lifting surface theory. The geometry is perturbed in such a manner that the pressure distribution on the perturbed surface satisfies a "target" distribution. Iteration is required because the pressure is a nonlinear function of the geometry perturbation. In each iteration cycle, there are two major steps: (a) an analysis solution of the geometry; in the first iteration, the analysis is performed on the baseline configuration; and (b) a modification of the geometry. The first step follows the analysis procedure already described. The modification of geometry in the second step is obtained, for example, by requiring that the pressure distribution on the modified contour satisfies a "target" distribution. The first-order Taylor series expansion of the velocity

potential about the baseline geometry requires knowledge of the partial derivatives of velocity potential with respect to the geometry coordinates. The partial derivatives are calculated once only and then are stored for repetitive use during the iteration procedure. Hawk and Bristow[30] reported that the perturbation analysis method is competitive in accuracy with that of conventional panel analysis methods, the computing cost of each successive application is one order of magnitude less, and the perturbation design method is efficient in calculating three-dimensional wing section geometry corresponding to a prescribed pressure distribution. Although the sample problems presented by Bristow[29] and Hawk[30] are wing-section related, the extension of the method to propeller blade design is straightforward.

SAMPLE CALCULATIONS

Lifting surface theory and equivalent two-dimensional theory have been used[31,32] to predict the pressure distribution on the surface of propeller blades. Neither theory accounts for the effect of the hub. Due to this limitation in design and analysis procedures, the hub effect is often greatly simplified or ignored. Detailed knowledge of the pressure distribution on the blade surface—especially around the leading edge—is important to cavitation inception prediction. However, neither theory performed satisfactorily, especially at the off-design conditions.

The panel method distributes the singularities on the surfaces of both the blade and the hub. A hub with any arbitrary shape can be easily modeled as an integrated part of a propeller. The geometry of the propeller unit can be modeled in as much detail as the maximum number of panels allows, avoiding the shortcoming suffered by the lifting surface theory.

Benchmark comparisons for the panel method calculations presented in this report were performed using the experimental results previously reported at the David Taylor Research Center (DTRC). Model tests were conducted with DTRC Propeller 4718 with a hub/diameter ratio of 0.3. The propeller drawing is shown in Fig. 3, with tabulated geometry listed in Table 1. The propeller was tested in an open jet test section of the DTRC 36-in. variable-pressure water tunnel and in open water in the DTRC high-speed towing basin. The measurements of the pressure on the blade surface were taken at locations that were 0.5, 0.7, 0.8, and 0.9 of the tip radius.

During the experiment,[33] an extensive calibration program was conducted to arrive at accurate calibrations for test purposes, and to investigate possible systematic errors in pressure measurement instrumentation. For any single calibration, the error band, based on a 95% confidence level, was calculated from the standard deviation relative to a straight line calculated sensitivity. It was determined that the uncertainty of pressure measurements at low test speed (6 knots) and at high test speed (11 knots) is ± 0.05 psi and ± 0.07 psi, respectively. The detailed method of calibration can be found in Reference 33.

The panel method[34-36] used in the calculations was the VSAERO code; it has piecewise constant source and doublet formation as described previously. The exact blade surface was approximated with 609 flat quadrilateral panels, and the hub was approximated with 144 panels. The panelized propeller is shown in Fig. 4.

To demonstrate the hub effect, the performances of the propeller without and with a hub were calculated. The results were then compared with predictions from lifting surface theory and with experimental data.

Comparisons were made between the measured surface pressure and predictions from the lifting surface theory and from the panel method without the hub. The results are shown in Fig. 5. In general, predictions using the panel method were an improvement over the lifting surface theory. However, predictions at the 0.5 radius were less than satisfactory. The large discrepancies between the predictions and experimental data were attributed to the hub effect that was not accounted for in the calculations.

With the hub model included, the pressure distributions were again calculated by the panel method, and the results are shown in Fig. 6. The agreement between the predictions and experimental data improved significantly, especially at the 0.5 radial section where the hub effect is expected to be great.

The fluid accelerates as it passes the hub and influences the flow at the blade sections. Locally, each blade section operates at an advance ratio that is different from, and greater than, the design value. The difference is greatest near the hub/blade junction and diminishes as the ratio r/R increases. Qualitatively, the hub increases the pressure near the leading edge and decreases the pressure near the trailing edge on the suction side and imposes the opposite effect on the pressure side. The panel method predicts this effect correctly, and the agreement with the experiment data is excellent.

Predictions of pressure distributions at off-design conditions were calculated, and comparisons with predictions from lifting surface theory and experimental data are shown in Figs. 7-9. The calculated pressure peaks at the leading edge agree well with the experimental data.

CONCLUSIONS

It is demonstrated here that the panel method is an improvement over lifting surface theory in predicting pressure distribution on propeller blade surface. The most significant improvements are that (a) the panel method can accommodate complicated hub geometry with relative ease and (b) it can provide more reliable information near the leading edge where many other approaches have failed, especially under off-design conditions. Although the formation of the panel code VSAERO is first order in nature, the results agree with the experimental data well. One computation (for a given advance coefficient J) requires 23 minutes CPU on a VAX/780 machine.

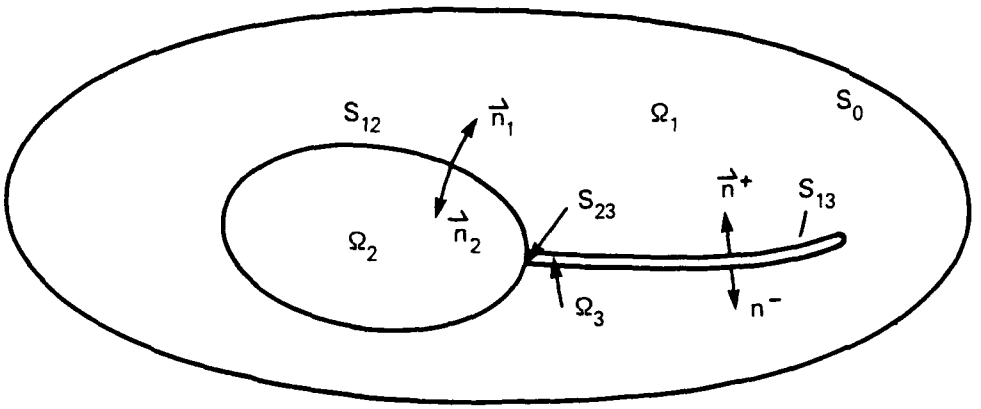

Fig. 1. Definition sketch of a generalized lifting body model.

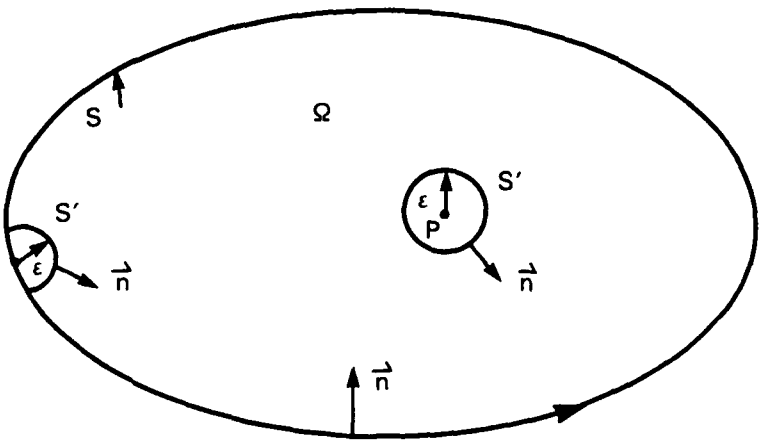

Fig. 2. Definition sketch of a singular point inside of the flow domain.

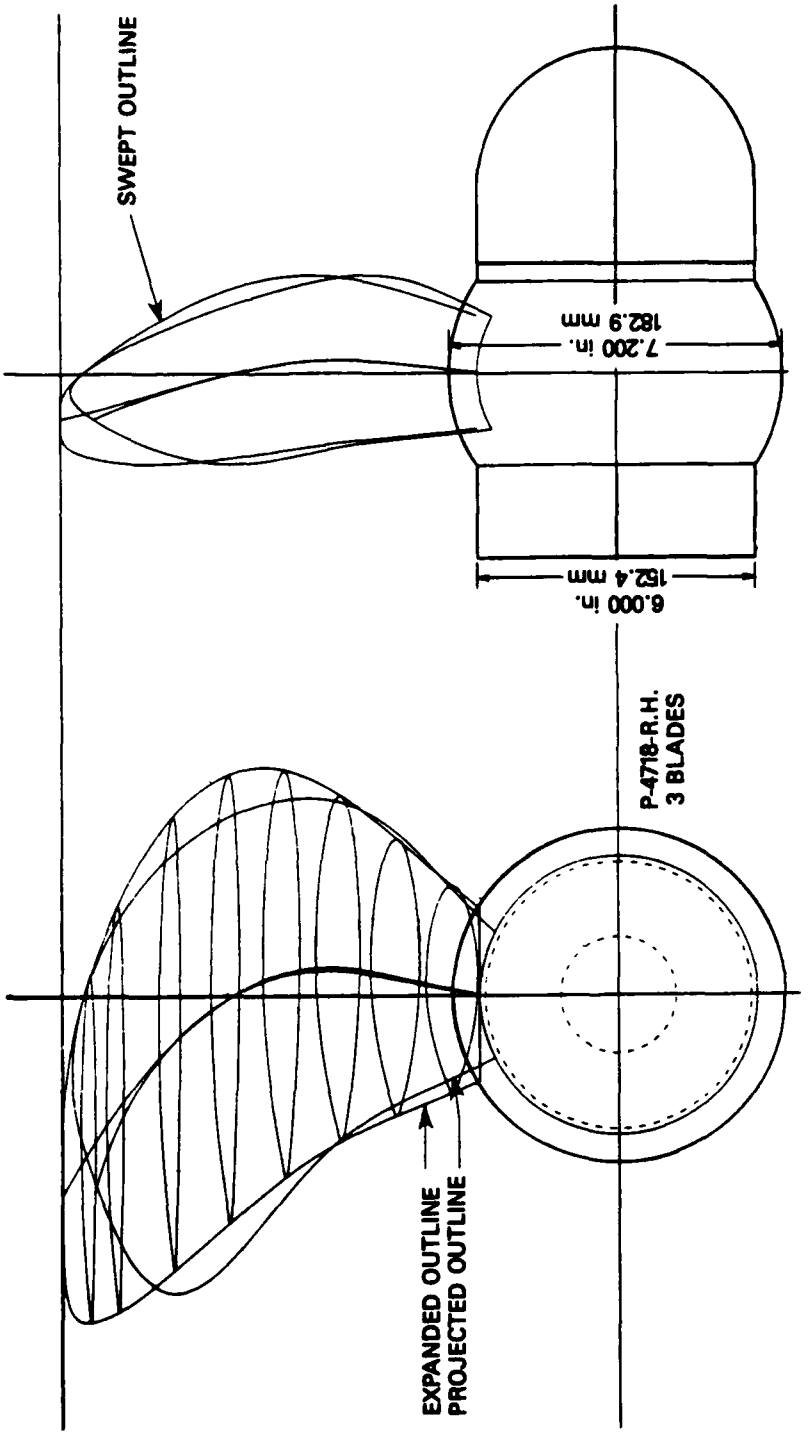

Fig. 3. DTRC Propeller 4718.

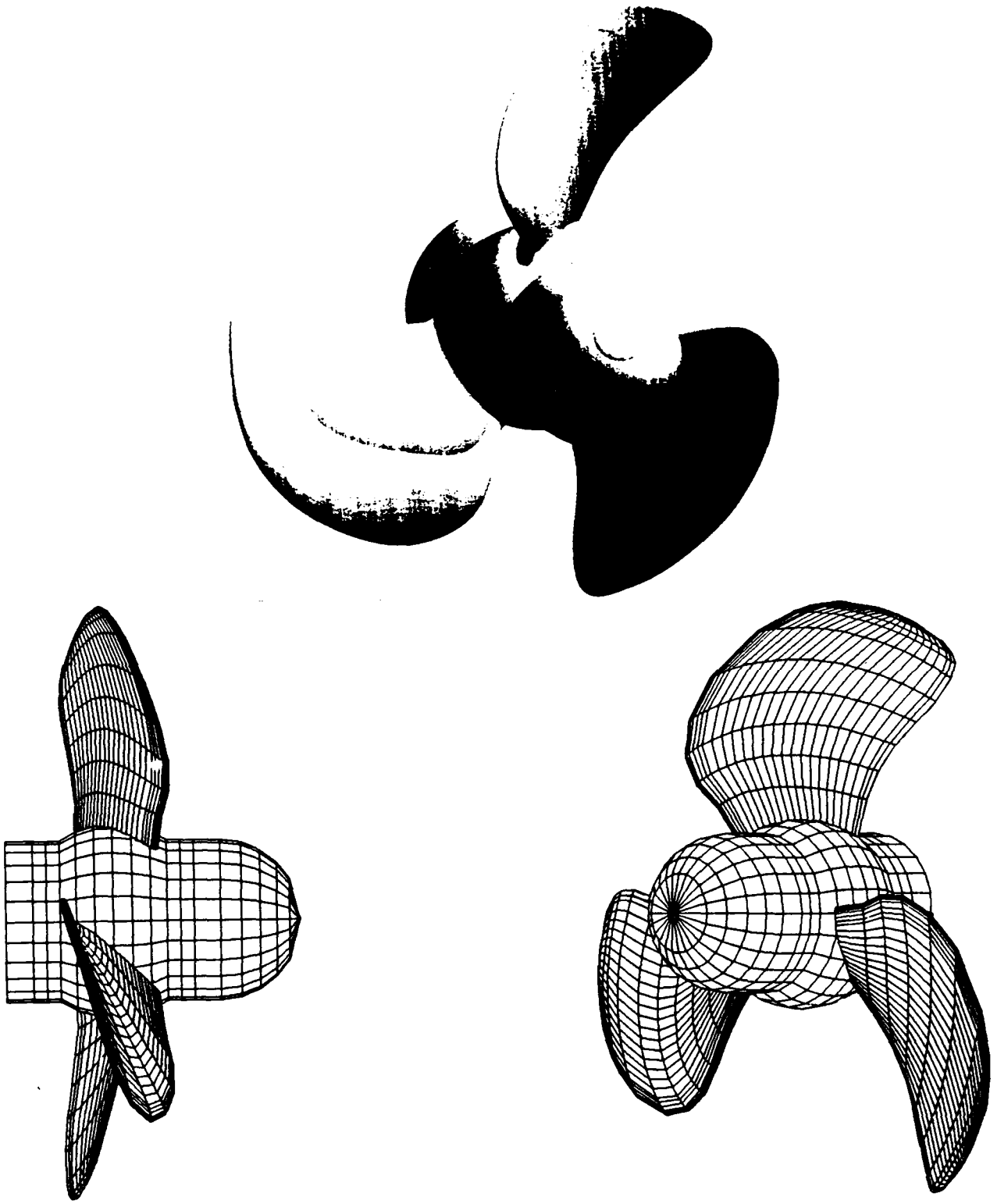

Fig. 4. Panelized propeller blade and hub.

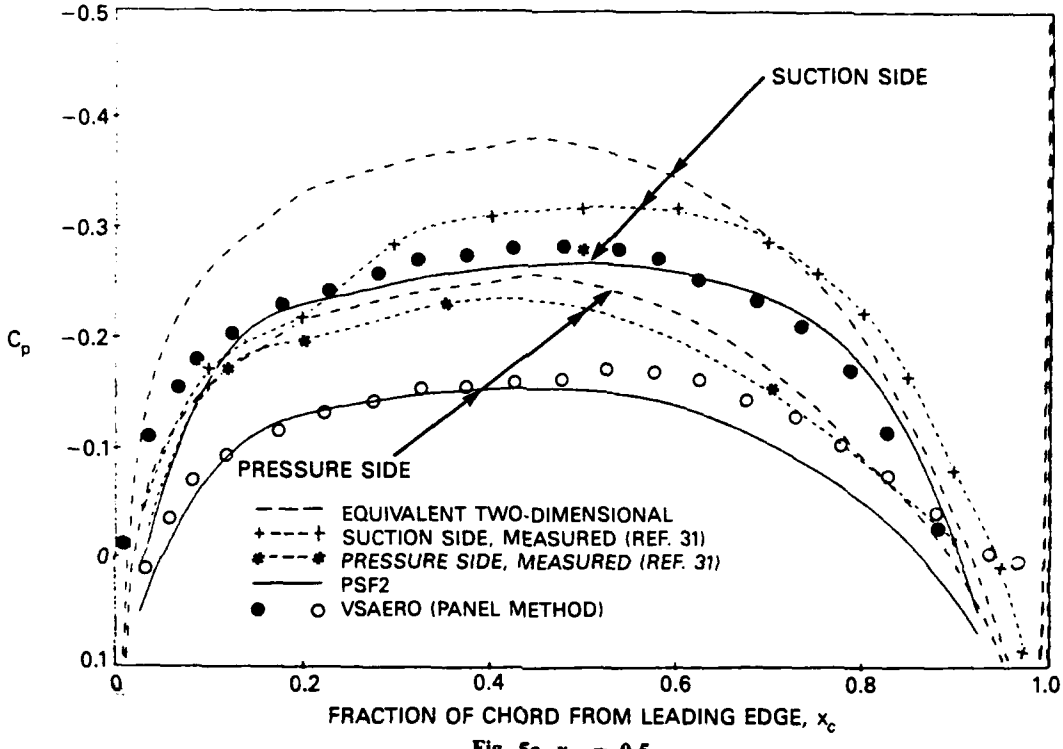

Fig. 5a. $x_R = 0.5$.

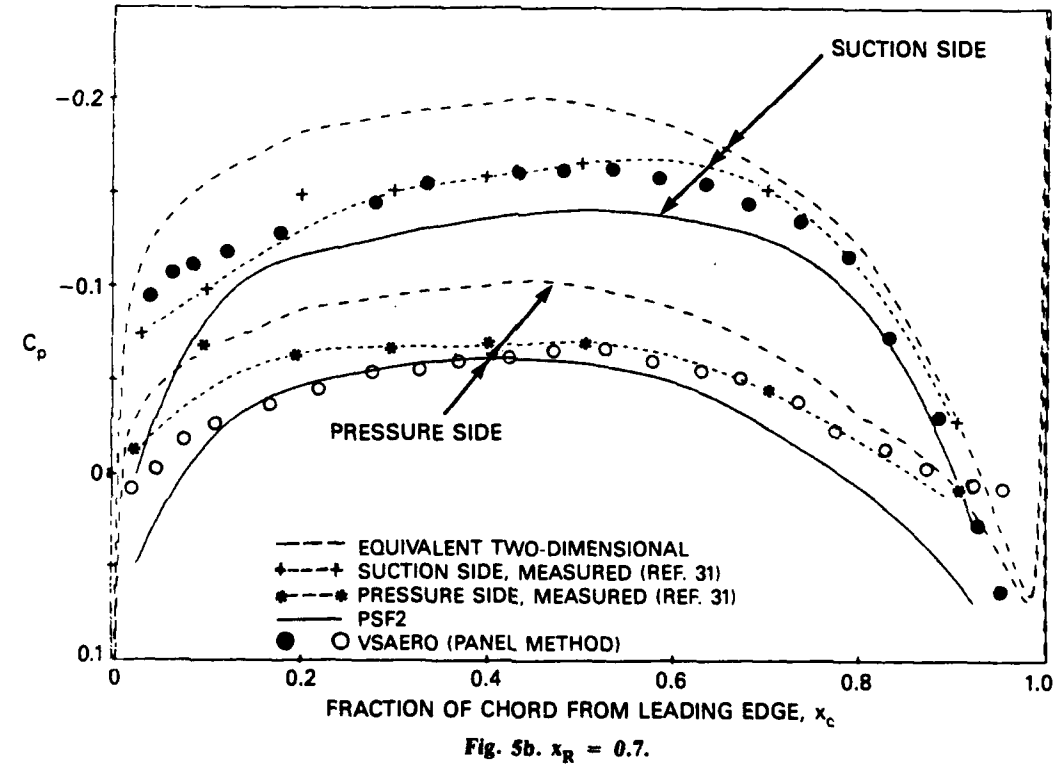

Fig. 5b. $x_R = 0.7$.

Fig. 5. Comparison of blade pressure measurement C_P with lifting surface theory and panel method calculations (without hub model) for Propeller 4718 at various fractions of propeller radius x_R.

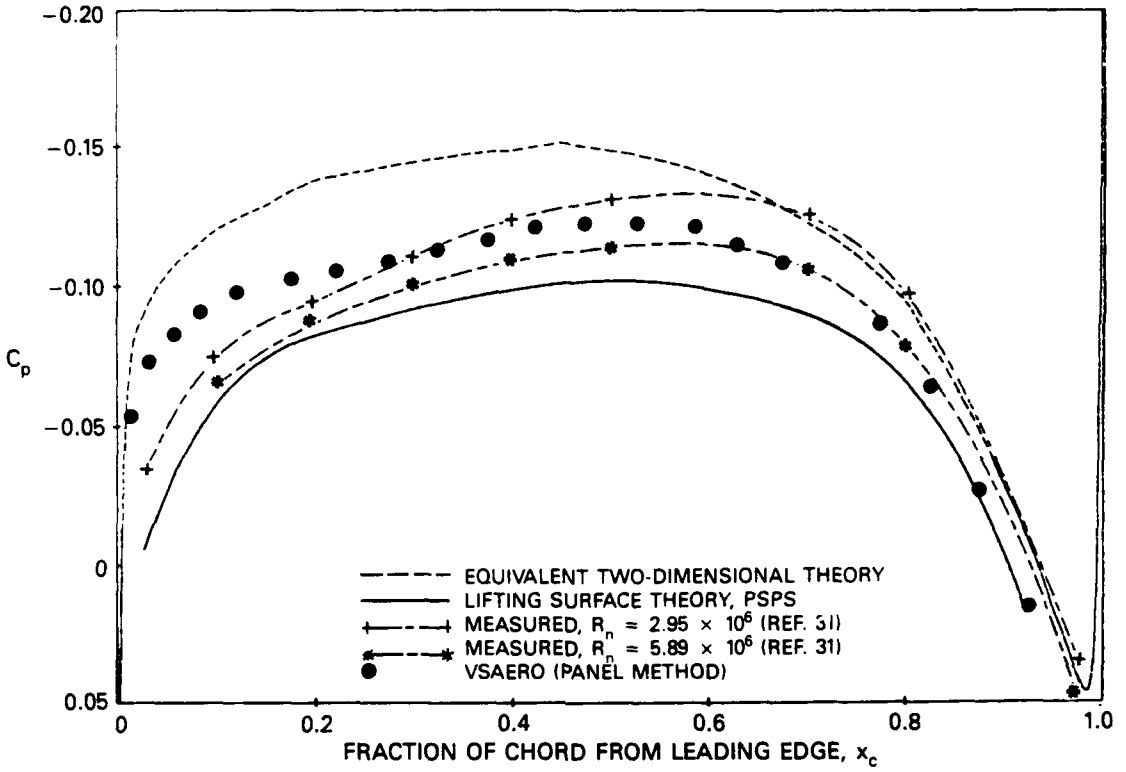

Fig. 5c. x_R = 0.8.

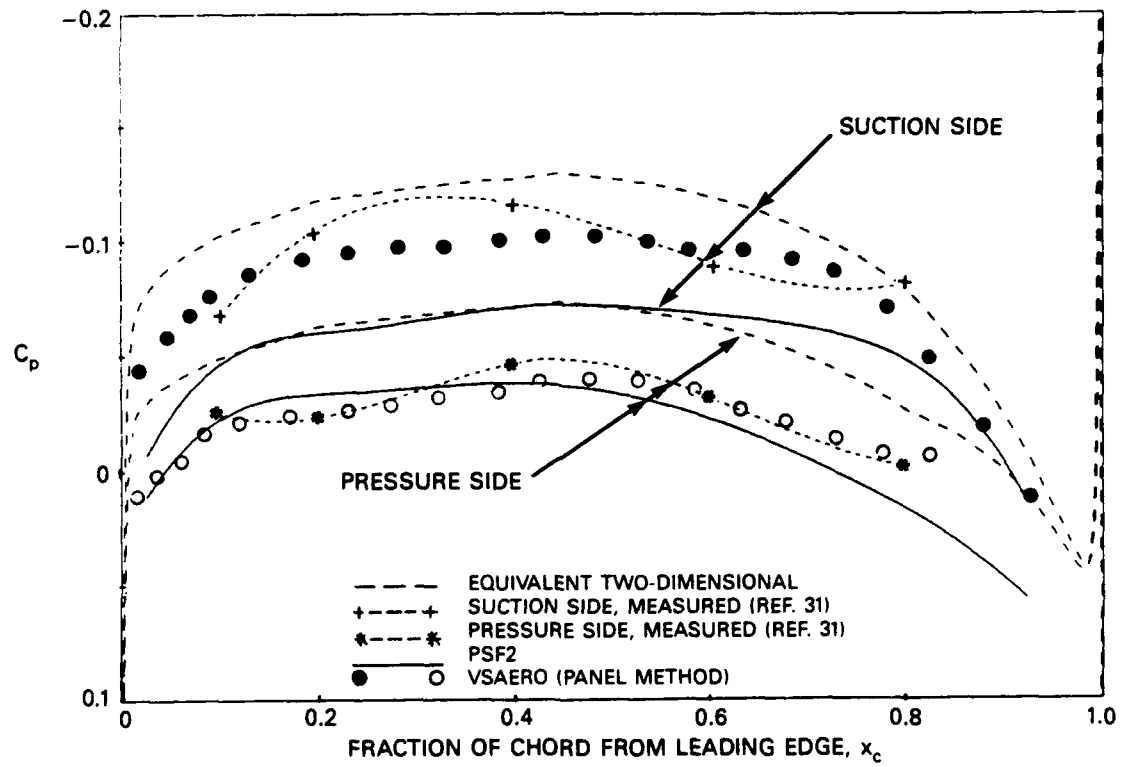

Fig. 5d. x_R = 0.9.

Fig. 5. (Continued)

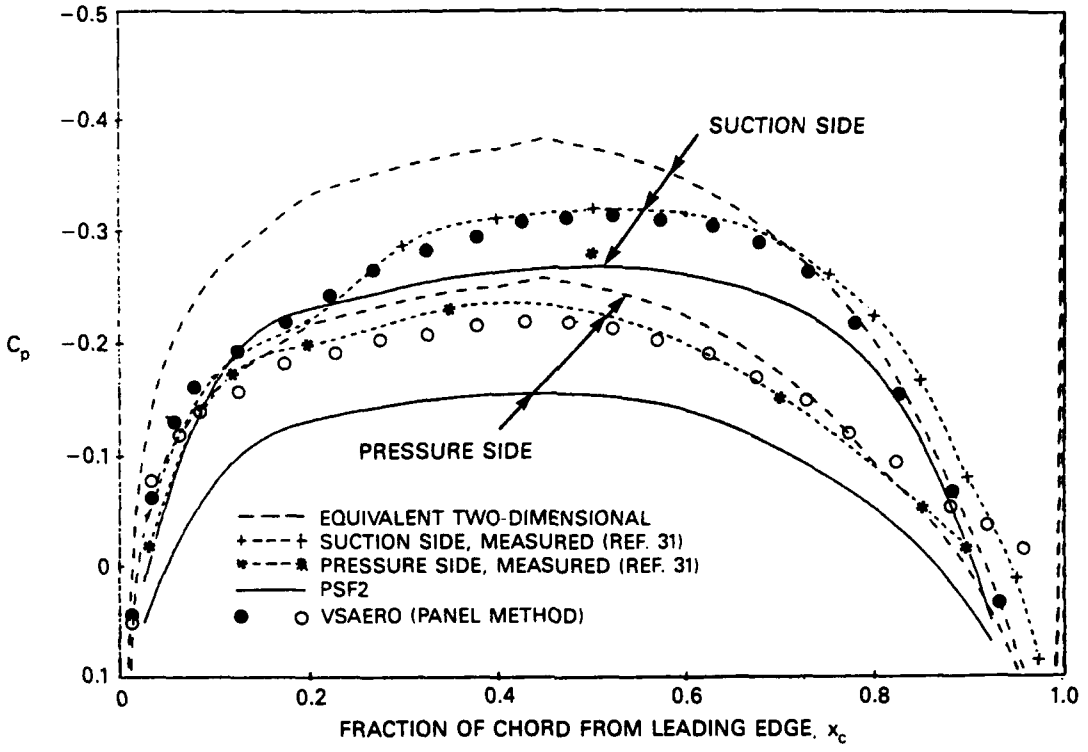

Fig. 6a. x_R = 0.5.

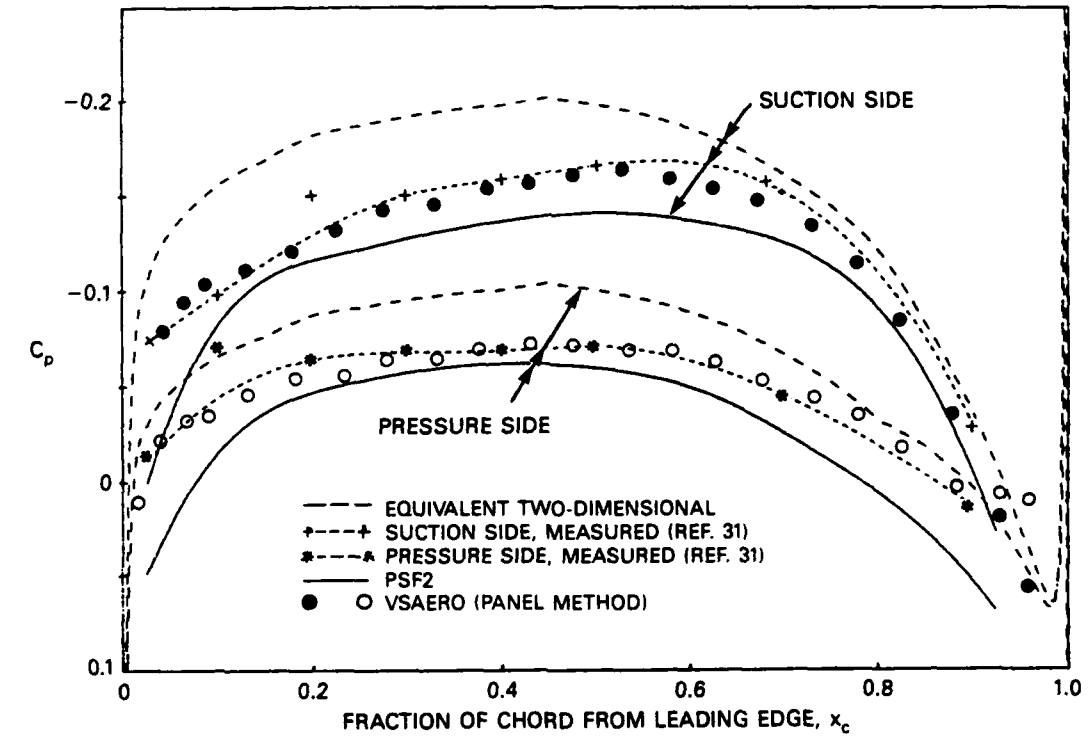

Fig. 6b. x_R = 0.7.

Fig 6. Comparison of blade pressure measurements C_P with lifting surface theory and panel method calculations (with hub model) for Propeller 4718 at various fractions of propeller radius x_R.

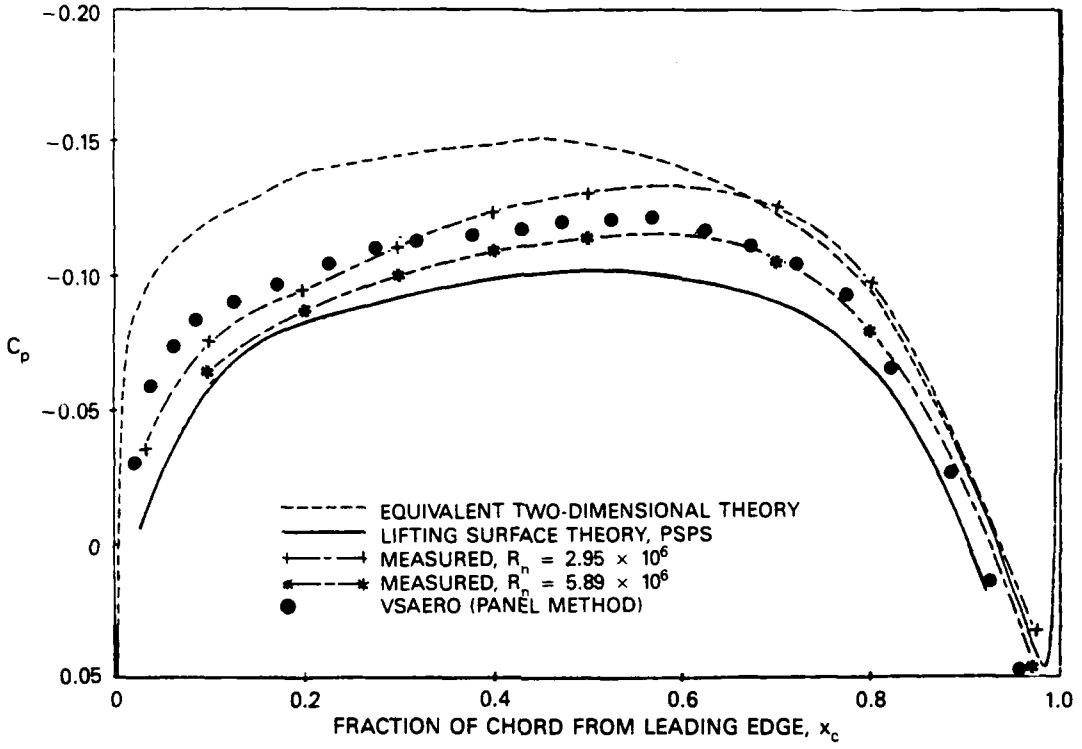

Fig. 6c. x_R = 0.8.

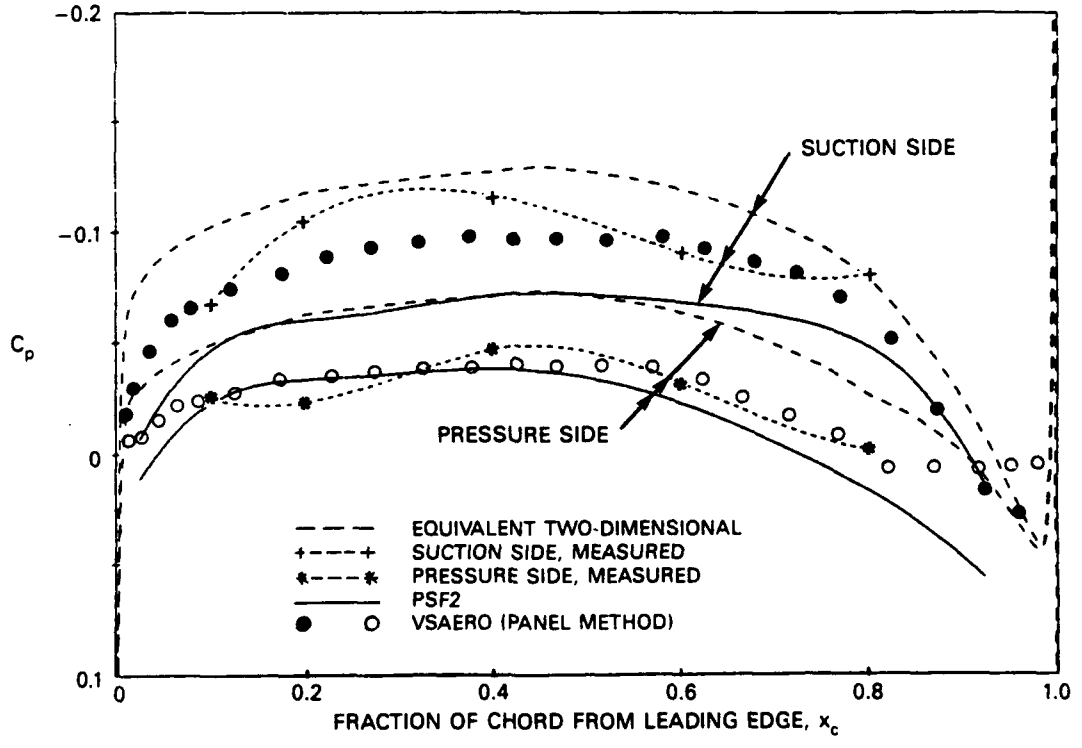

Fig. 6d. x_R = 0.9.

Fig. 6. (Continued)

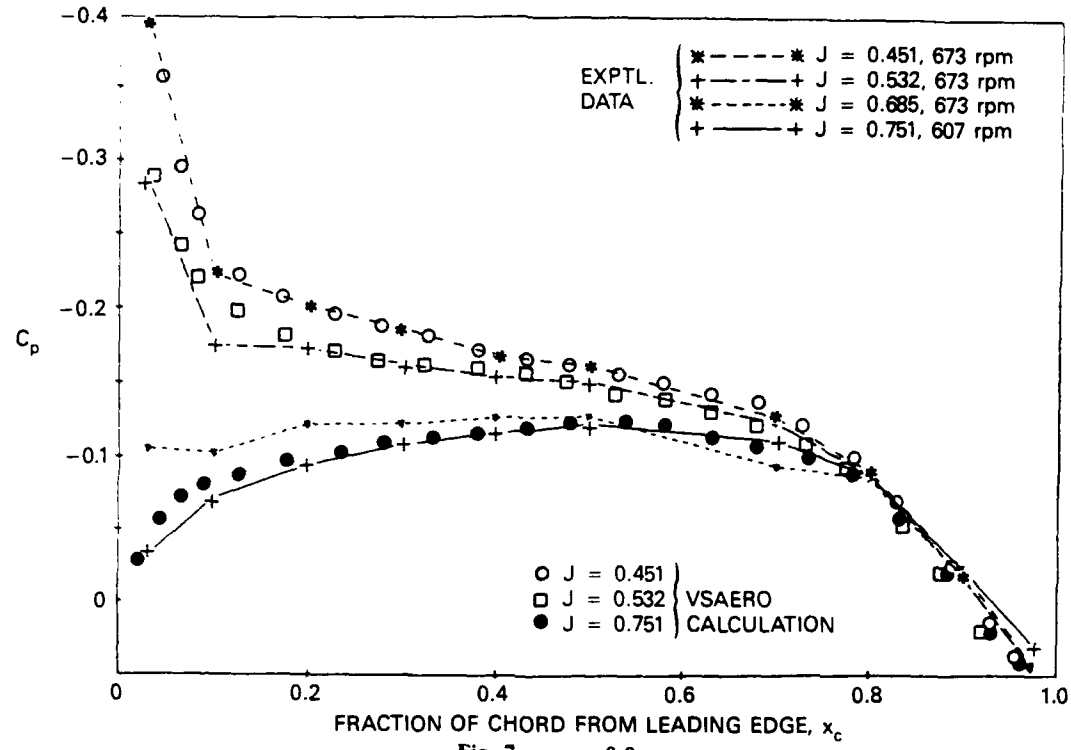

Fig. 7a. $x_R = 0.8$.

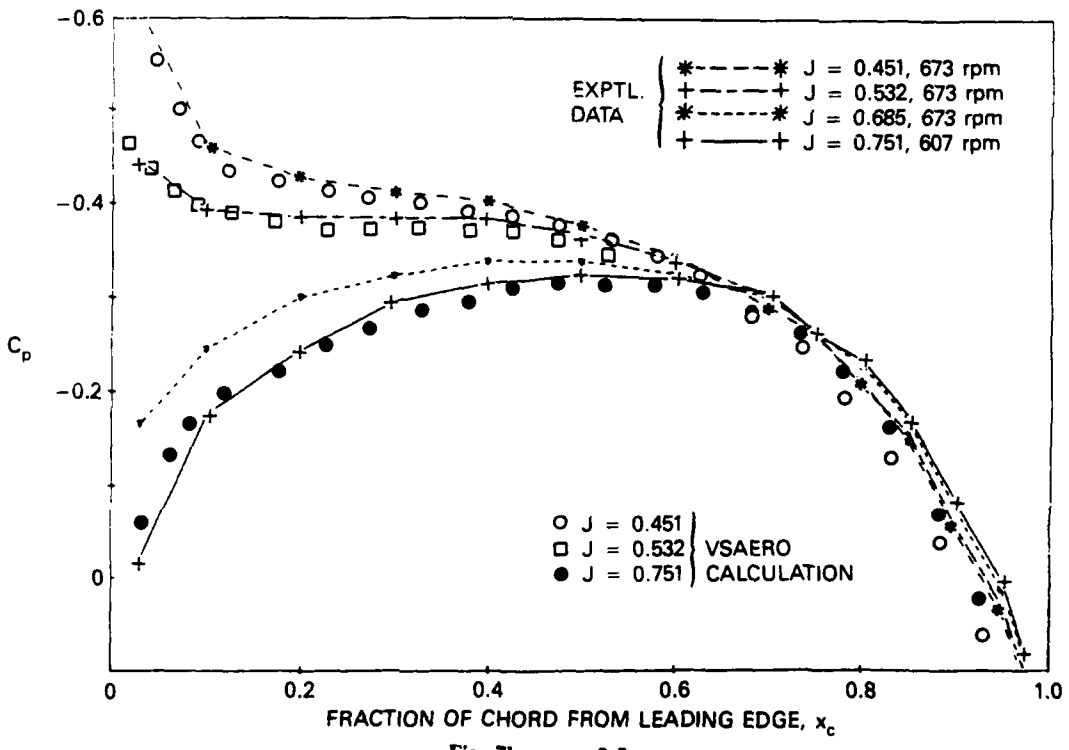

Fig. 7b. $x_R = 0.5$.

Fig. 7. Off-design pressure distributions C_P on the suction side of Propeller 4718 for various fractions of propeller radius x_R.

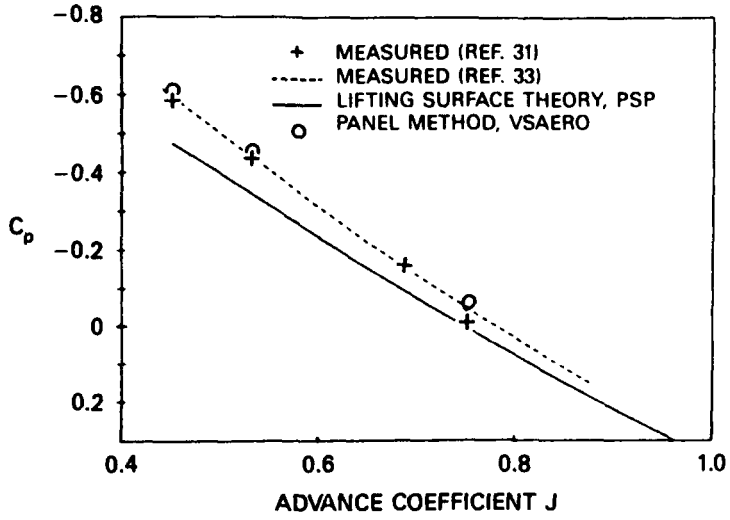

Fig. 8a. $x_c = 0.03$.

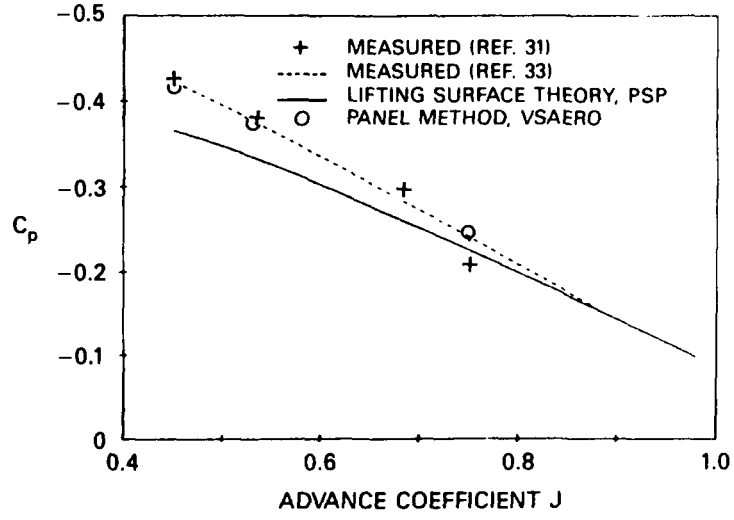

Fig. 8b. $x_c = 0.2$.

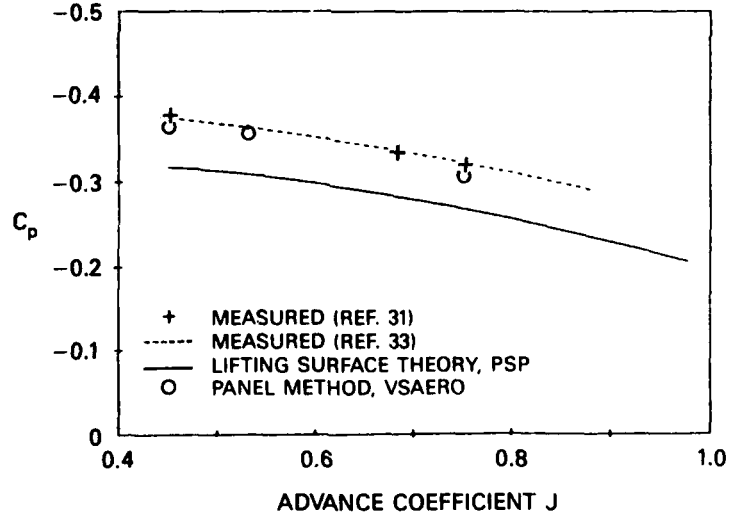

Fig. 8c. $x_c = 0.5$

Fig. 8. Variation of pressure distribution C_P with the advance coefficient J. Comparison with lifting surface theory and panel method calculations for $x_R = 0.5$ at various fractions of chord x_c.

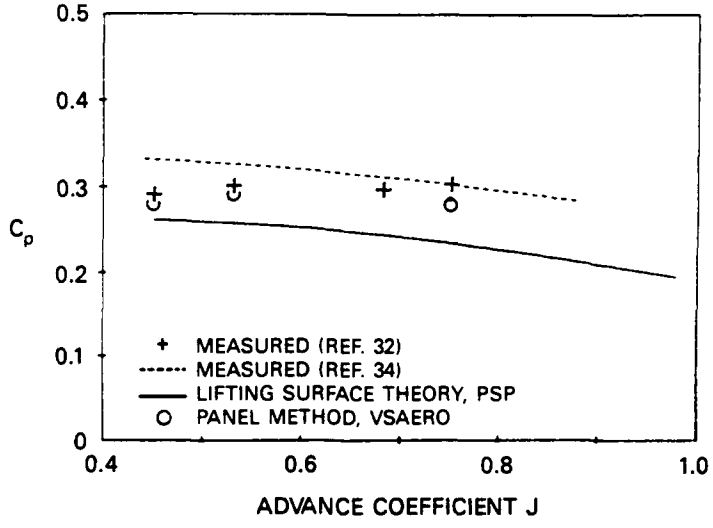

Fig. 8d. x_c = 0.7.

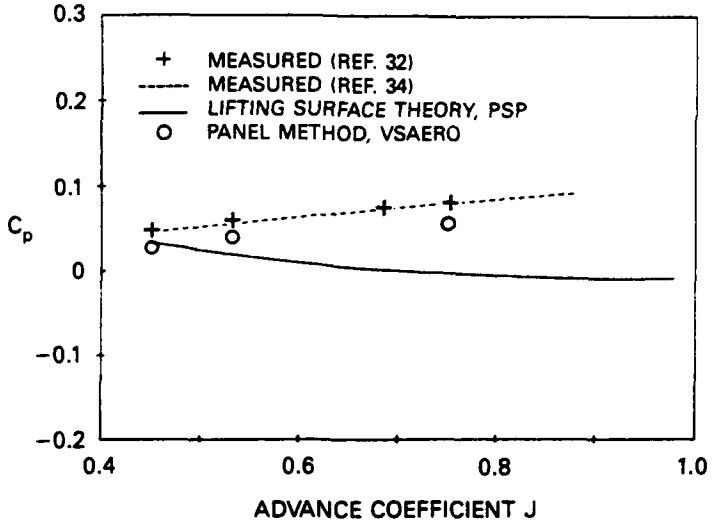

Fig. 8e. x_c = 0.9.

Fig. 8. (Continued)

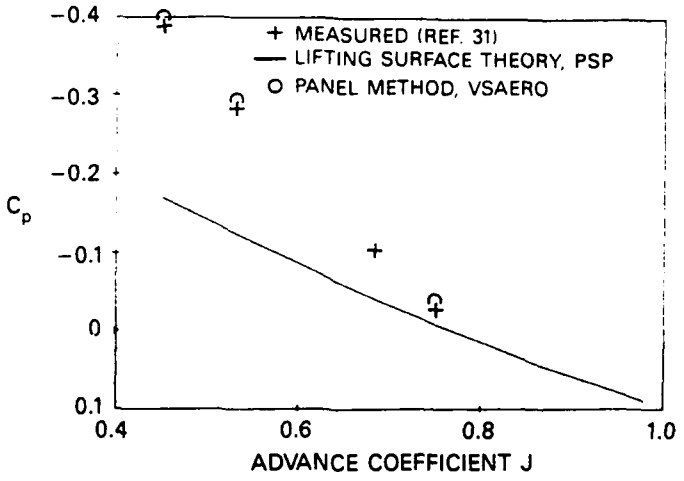

Fig. 9a. x_c = 0.03.

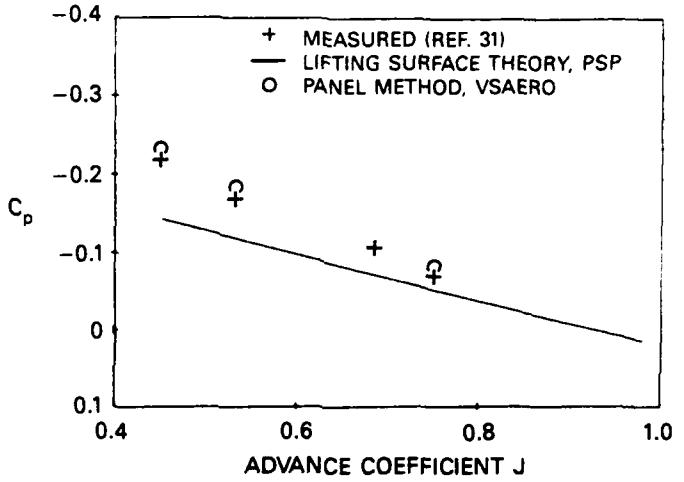

Fig. 9b. x_c = 0.1.

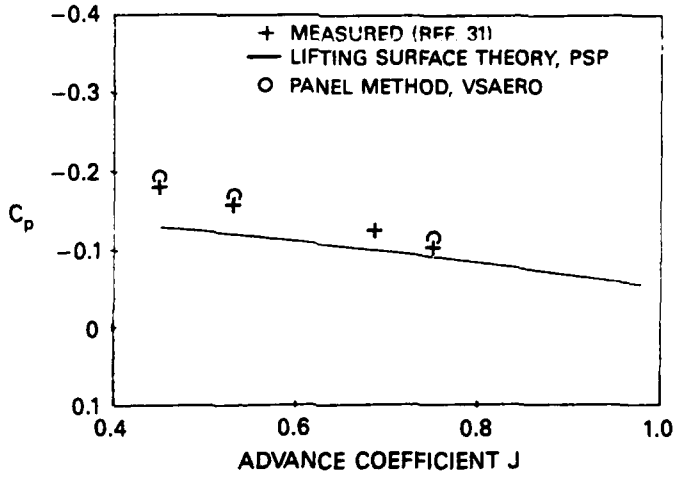

Fig. 9c. x_c = 0.3

Fig. 9. Variation of pressure distribution C_P with the advance coefficient J. Comparison with lifting surface theory and panel method calculations for x_R = 0.8 at various fractions of chord x_c.

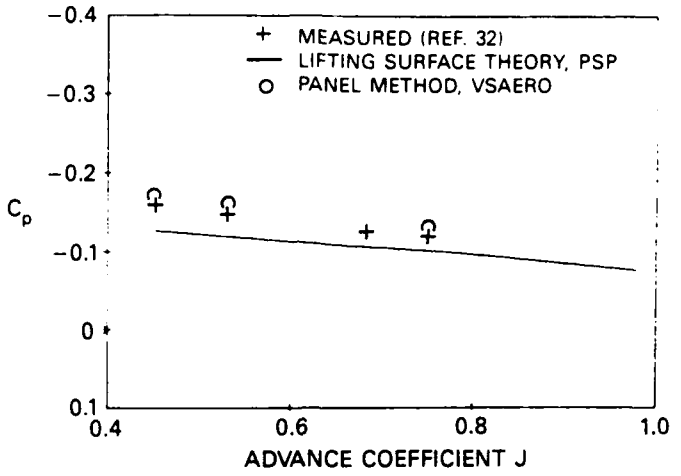

Fig. 9d. x_c = 0.5.

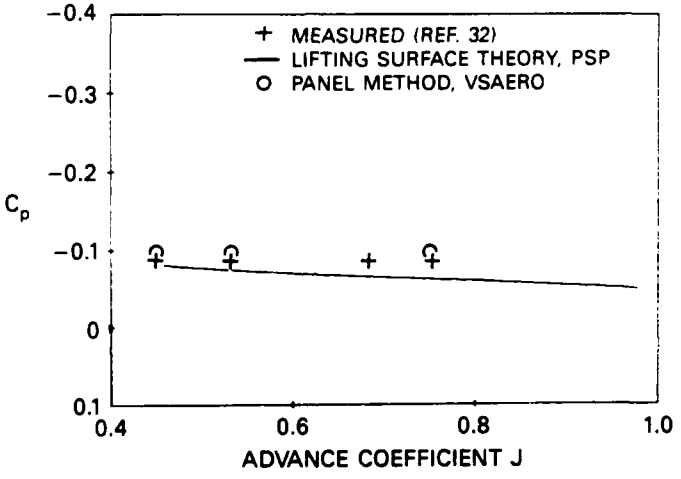

Fig. 9e. x_c = 0.8.

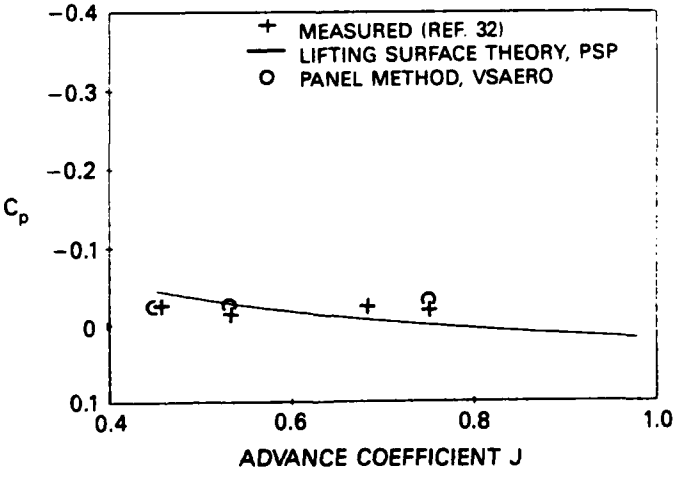

Fig. 9f. x_c = 0.9.

Fig. 9. (Continued)

Table 1. Properties of Propeller 4718.

Blade Geometry & Design

Diameter D = 2.000 ft (0.610 m)	Blade Thickness Fraction = 0.069
Rotation = Right Hand	Design Advance Coefficient J = 0.751
Number of Blades Z = 3	Design Thrust Loading Coefficient C_{Th} = 0.248
Hub/Diameter Ratio D_h/D = 0.30	Design Thrust Coefficient K_T = 0.055
Expanded Area Ratio = 0.44	Design Torque Coefficient K_Q = 0.0106

Blade Parameters

r/R	c/D	P/D	θ_s (deg)	i_G/D	t/c	t/D	f_M/c	f_M/D
0.3	0.187	0.718	-1.65	0.0	0.2497	0.0467	0.0	0.0
0.4	0.249	0.796	-4.05	0.0	0.1771	0.0441	0.0044	0.0011
0.5	0.311	0.855	-5.00	0.0	0.1280	0.0398	0.0085	0.0027
0.6	0.366	0.886	-3.50	0.0	0.0910	0.0333	0.0099	0.0036
0.7	0.403	0.888	0.40	0.0	0.0630	0.0254	0.0101	0.0041
0.8	0.409	0.870	5.75	0.0	0.0469	0.0192	0.0097	0.0090
0.9	0.365	0.825	12.40	0.0	0.0419	0.0153	0.0082	0.0030
0.95	0.311	0.786	16.10	0.0	0.0418	0.0130	0.0065	0.0020
1.0	0.070	0.734	20.00	0.0	0.0414	0.0029	0.0090	0.0006

Thickness & Camber Distribution

x_c	E_T/t*	E_c/f_M†
0.0000	0.0000	0.0000
0.005	0.0665	0.0423
0.0075	0.0812	0.0595
0.0125	0.1044	0.0907
0.025	0.1466	0.1586
0.05	0.2066	0.2712
0.075	0.2525	0.3657
0.1	0.2907	0.4482
0.15	0.3521	0.5869
0.2	0.4000	0.6993
0.25	0.4363	0.7905
0.3	0.4367	0.8635
0.35	0.4832	0.9202
0.4	0.4952	0.9615
0.45	0.5	0.9881
0.5	0.4962	1.0
0.55	0.4846	0.9971
0.6	0.4653	0.9786
0.65	0.4383	0.9434
0.7	0.4035	0.8892
0.75	0.3612	0.8121
0.8	0.3110	0.7027
0.85	0.2532	0.5425
0.9	0.1877	0.3586
0.95	0.1143	0.1713
0.975	0.0748	0.0823
1.0	0.0333	0

* NACA 66 section (DTNSRDC modified).

† NACA a = 0.8 meanline: the design procedure determines the magnitude of the camber at each radius and uses the two-dimensional chordwise distribution of camber.

APPENDIX

A fluid is incompressible if its particles maintain their density along their paths, i.e., the substantial derivative of mass density ϱ is zero:

$$\frac{D\varrho}{Dt} = 0. \tag{A.1}$$

The principle of mass conservation requires that the net amount of mass flow into a control volume per unit time be equal to the rate at which the mass in the control volume is increasing. Thus

$$\frac{\partial \varrho}{\partial t} + \nabla \cdot \varrho \mathbf{u} = 0. \tag{A.2}$$

Equation A.1 is the differential equation of continuity. The bold type denotes a vector quantity J. From Eqs. A.1 and A.2 it follows that for incompressible fluids the equation of continuity is simply

$$\nabla \cdot \mathbf{u} = 0, \tag{A.3}$$

Whether or not the flow is steady and whether or not the fluid is homogeneous. Furthermore, if the flow is irrotational, the circulation around a closed circuit is zero,

$$\int \mathbf{u} \cdot d\mathbf{x} = 0. \tag{A.4}$$

Therefore, $\mathbf{u} \cdot d\mathbf{x}$ is an exact differential, which can be denoted by $d\Phi$, thus

$$\mathbf{u} = \nabla \Phi. \tag{A.5}$$

Equations A.3 and A.5 imply that the function Φ satisfies the Laplace equation,

$$\nabla^2 \Phi = 0. \tag{A.6}$$

Equation A.6 is a kinematic condition; velocity components can be obtained from its solution. The associated pressure, however, can be obtained only from a dynamic condition, that is, the equation of motion. For propeller application, it is more convenient tc express the equation of motion with respect to a rotating frame that is fixed to the propeller axis. If the fluid is inviscid and the reference frame is rotating with a constant angular velocity ω about the x axis, Newton's second law governing the flow becomes

$$\frac{D\mathbf{u}}{Dt} + \mathbf{F}_c = -\frac{1}{\varrho}\nabla\varrho - \nabla\left(\Omega - \frac{\omega^2 r^2}{2}\right), \tag{A.7}$$

where $\mathbf{F}_c$ is the Coriolis acceleration vector, Ω is the body force potential, and $r^2 = y^2 + z^2$.

The Coriolis acceleration vector F_c $(0, -2\omega w, 2\omega v)$ is perpendicular to the velocity vector (u, v, w). Hence its projection onto a streamline is zero. If the flow is steady, then along a streamline s the equation of motion becomes

$$u_2 \frac{\partial u_s}{\partial S} = - \frac{\partial}{\partial S} \left(\int \frac{\partial P}{\varrho} + \Omega - \frac{\omega^2 r^2}{2} \right) . \tag{A.8}$$

If ϱ is constant, integration of Eq. A.8 yields

$$\frac{P}{\varrho} + \frac{u_s^2}{2} + \Omega - \frac{\omega^2 r^2}{2} = \text{constant along a streamline.} \tag{A.9}$$

The constant on the right-hand side of Eq. A.9 can be determined by the upstream condition.

In summary, to derive at Eqs. A.6 and A.9, it was assumed that (1) the fluid is incompressible and inviscid, and (2) the flow is irrotational and steady. As a consequence, the flow solutions can be obtained from Eqs. A.6 and A.9 instead of from Eqs. A.2 and A.7. (Equations A.6 and A.9 are simplified forms of Eqs. A.2 and A.7.) Equation A.6 is linear with linear boundary conditions (without free surface); it can be solved very easily. The velocity components can be determined from Eq. A.5, and the associated pressure calculated from Eq. A.9. The nonlinearity of Eq. A.7 is reflected only in the nonlinearity of Eq. A.9, and there it presents no difficulty at all because the nonlinear term is clearly determined and only the pressure is to be evaluated.

REFERENCES

1. Hess, J.L., and A.M.O. Smith, "Calculation of Potential Flow about Arbitrary Bodies," *Prog. in Aero. Sci.,* Pergamon Press, New York (1966), p. 1.
2. Hess, J.L., "The Problem of Three-Dimensional Lifting Flow and Its Solution by Means of Surface Singularity Distribution," *Computer Methods in Applied Mechanics and Engineering,* Vol. 4, p. 283 (Nov 1974).
3. Rubberts, P.E., and G.R. Saaris, "Review and Evaluation of a Three-Dimensional Flow Analysis Method for Arbitrary Configurations," American Institute of Aeronautics and Astronautics (AIAA) Paper No. 72-188 (1972).
4. Morino, L., and C.C. Kuo, "Subsonic Potential Aerodynamics for Complex Configurations: A General Theory," *AIAA Journal,* Vol. 12, No. 2, p. 191 (Feb 1974).
5. Vaidyanathan, T.S., B. Maskew, and F.A. Dvorak, "The Application of Advanced Nonlinear Panel Methods to the Analysis of Marine Propellers," AMI Report 8404 (Mar 1984).
6. Hess, J.L., "Calculation of Steady Flow About Propellers Using a Surface Panel Method," *J. Propulsion,* Vol. 1, No. 6, p. 470 (Dec 1985).
7. Batchelor, G.K., *An Introduction to Fluid Dynamics,* Cambridge University Press (1967).
8. Johnson, F.T., and P.E. Rubbert, "Advanced Panel-Type Influence Coefficient Methods Applied to subsonic Flows," *Proceedings of AIAA 13th Aerospace Science Meeting* (Jan 1975).
9. Bristow, D.R., and G.G. Grose, "Modification of the Douglas Neumann Program to Improve the Efficiency of Predicting Component Interference and High Lift Characteristics," NASA Contract Report CR-3020 (1978).
10. Maskew, B., "Influence of Rotor Blade Tip Shape on Tip Vortex Shedding—an Unsteady, Inviscid Analysis," Presented at the 36th Annual Forum of the American Helicopter Society, Washington, D.C. (May 1980).
11. Hess, J.L., "Calculation of Potential Flow About Arbitrary Three-Dimensional Lifting Bodies," McDonnell Douglas Corporation Report MDC J5679-01, McDonell Douglas (Oct 1972).
12. Cebeci, T., K. Stewartson, and J.H. Whitelaw, "Calculation of Two-Dimensional Flow Past Airfoils," *Numerical and Physical Aspects of Aerodynamic Flows,* (ed. by T. Cebeci), Vol. 2, p. 1 (1983).
13. Mahgoub, H.E.H., and P. Bradshaw, "Calculation of Turbulent-Inviscid Flow Interactions with Large Normal Pressure Gradients," *AIAA Journal,* Vol. 17, No. 10, p. 1025 (1979).
14. Le Balleur, J.C., "Strong Matching Method for Computing Transonic viscous Flows Including Wakes and Separations," *La Recherche Aerospatiale,* No. 1981-3, p. 21, (English translation).
15. Kline, S.J., B.J. Cantwell, and G.M. Lilley, (eds.) *"Proceeding of 1980-1981 AFOSR-HTTM Stanford Conference on Complex Turbulent Flow,"* Stanford University (1981).

16. Dutt, H.N.V., and A.K. Sreekanth, "Design of Aerofoils for Prescribed Pressure Distribution in Viscous Incompressible Flows," *Aero. Quant.*, p. 42 (Feb 1980).

17. Lighthill, M.J. "On Displacement Thickness," *J. Fluid Mech.*, 4, p. 383 (1958).

18. Green, J.E., D.W. Weeks, and J.W.F. Brooman, "Prediction of Turbulent Boundary Layers and Wakes in Compressible Flow by a Lag Entrainment Method," Royal Aircraft Establishment (RAE) Report TR 72231, (1972).

19. East, L.F., P.D. Smith, and P.J. Merryman, "Prediction of the Development of Separated Turbulent Boundary Layers by the Lag-entraiment Method,' Royal Aircraft Establishment (RAE) Report TR 77046 (1977).

20. Lock, R.C., and M.C.P. Firmin, "Survey of Techniques for Estimating Viscous Effects in External Aerodynamics," *Numerical Methods in Aeronautical Fluid Dynamics,* ed. by P.L. Roe, Academic Press (1983), p. 337.

21. Melnik, R.E., and J.W. Brook, "The Computation of Viscid/Inviscid Interaction on Airfoils with Separated Flow," *Third Symposium on Numerical and Physical Aspects of Aerodynamic Flow,* (1985), pp. 1-21.

22. Dvorak, F.A., B. Maskew, and F.A. Woodward, "Investigation of Three-Dimensional Flow Separation on Fuselage Configuration," US Army AMRDL Rept. TR-77-4, (Mar 1977).

23. Dvorak, F.A., F.A. Woodward, and B. Maskew, "A Three-Dimensional Viscous/Potential Flow Interaction Analysis Method for Multi-Element Wings," NASA CR-152012 (Jul 1977).

24. Maskew, B., B.M. Rao, and F.A. Dvorak, "Prediction of Aerodynamic Characteristics for Wings with Extensive Separations," Paper No. 31 in Computation of Visccus-Inviscid Interactions, Advisory Group for Aerospace Research and Development (AGARD) Report CP-291 (Feb 1981).

25. Franc, J.P., and J.M. Michel, "Attached Cavitation and the Boundary Layer: Experimental Investigation and Numerical Treatment," *J. Fluid Mech.*, Vol. 154, pp. 63-90 (1985).

26. Fronasier, L., "Wing Design Process by Inverse Potential Flow Computer Program," *The Use of Computers as a Design Tool,* AGARD Report CP-280, (Sept 1979).

27. Johnson, F.T., "A General Panel Method for the Analysis and Design of Arbitary Configurations in Incompressible Flows," NASA Report CR-3079 (May 1980).

28. Slooff, J.W., "A Survey of Computational Methods for Subsonic and Transonic Aerodynamic Design," National Aerospace Laboratory, the Netherlands, Report MP84066 U (1984).

29. Bristow, D.R., and J.D. Hawk, "Subsonic 3-D Surface Panel Method for Rapid Analysis of Multiple Geometry Perturbation," American Institute of Aeronautics and Astronautics (AIAA), Report 82-0993 (1982).

30. Hawk, J.D., and D.R. Bristow, "Subsonic Surface Panel Method for Airframe Analysis and Wing Design," American Institute of Aeronautics and Astronautics (AIAA), Report 83-0341 (1983).

31. Jessup, S.D., "Further Measurements of Model Propeller Pressure Distributions Using a Novel Technique," DTNSRDC Report 86/011 (May 1986).

32. Kim, K-H, and S. Kobayashi, "Pressure Distribution on Propeller Blade Surface Using Numerical Lifting Surface Theory," *DTNSRDC Report* 84/072 (Jan 1985).

33. Jessup, S.D., "Measurement of the Pressure Distribution on Two Model Propellers," DTNSRDC Report 82/035 (Jul 1982).

34. Kerwin, J.E., Kinnas, S.A., Lee, J-T., Shih, W-Z., "A Surface Panel Method for the Hydrodynamic Analysis of Ducted Propellers," SNAME Annual Meeting Paper No. 4 (Nov 1987).

35. Yang, C-I., Jessup, S.D., "Benchmark Analysis of a Series of Propellers with a Panel Method," SNAME Propeller '88 Symposium, Virginia Beach, VA, Sep. 20-21, 1988.

36. Hoshino, T., "Hydrodynamic Analysis of Propellers in Steady Flow Using a Surface Panel Method," Presented at the Spring Meeting of the Society of Naval Architects of Japan, May 1989.

THIS PAGE INTENTIONALLY LEFT BLANK

INITIAL DISTRIBUTION

Copies	
12	DTIC

CENTER DISTRIBUTION

Serials	Code	Name
1	0117	B. Nakonechny
1	0120	
1	12	
1	15	W. B. Morgan
1	1506	D. Walden
1	1508	R. Boswell
1	152	W.–C. Lin
1	1521	W. Day
1	1521	G. Karafiath
1	1521	R. Hurwitz
1	1522	M. Wilson
1	154	J. McCarthy
1	1542	T. Huang
10	1544	C.–I. Yang
1	342.1	TIC (C)
1	342.2	TIC (A)
10	3432	Reports Control